REPORT NO. DOT-TSC-RSPA-79-17

THE AERODYNAMICS OF TRACKED RAM AIR CUSHION VEHICLES - EFFECTS OF PITCH ATTITUDE AND UPPER SURFACE FLOW

U.S. DEPARTMENT OF TRANSPORTATION
Research and Special Programs Administration
Transportation Systems Center
Cambridge MA 02142

PRINCETON UNIVERSITY
Department of Mechanical and Aerospace Engineering
Princeton NJ 08540

OCTOBER 1979

FINAL REPORT

DOCUMENT IS AVAILABLE TO THE PUBLIC THROUGH THE NATIONAL TECHNICAL INFORMATION SERVICE, SPRINGFIELD, VIRGINIA 22161

Prepared for

U.S. DEPARTMENT OF TRANSPORTATION
RESEARCH AND SPECIAL PROGRAMS ADMINISTRATION
Office of Transportation Programs Bureau
Washington DC 20590

Technical Report Documentation Page

1. Report No.	2. Government Accession No.	3. Recipient's Catalog No.
DOT-TSC-RSPA-79-17		

4. Title and Subtitle	5. Report Date
THE AERODYNAMICS OF TRACKED RAM AIR CUSHION VEHICLES - EFFECTS OF PITCH ATTITUDE AND UPPER SURFACE FLOW	October 1979
	6. Performing Organization Code
7. Author(s)	8. Performing Organization Report No.
T.M. Barrows,† H.C. Curtiss, Jr.,* W.F. Putman*	DOT-TSC-RSPA-79-17 MAE Technical Report 1426
9. Performing Organization Name and Address	10. Work Unit No. (TRAIS)
Princeton University* Department of Mechanical and Aerospace Engineering Princeton NJ 08540	RS906/R0508
	11. Contract or Grant No.
	DOT-TSC-682
12. Sponsoring Agency Name and Address	13. Type of Report and Period Covered
U.S. Department of Transportation Research and Special Programs Administration Office of Transportation Programs Bureau Washington DC 20590	Final Report Sep. 1973 - Feb. 1979
	14. Sponsoring Agency Code

15. Supplementary Notes

*Under contract to:

†U.S. Department of Transportation
Research and Special Programs Administration
Transportation Systems Center
Cambridge MA 02142

16. Abstract

Three types of experiments were conducted on geometrically similar models of a Tracked Ram Air Cushion Vehicle (TRACV). The first consisted of wind tunnel tests with the vehicle model positioned within a short segment of stationary guideway. In the second series of tests, the vehicle model was towed through a 300-foot guideway and the equilibrium position was measured as a function of model weight and center-of-gravity location. Techniques for deriving stability information from these data are described. The third type of test utilized a moving carriage which held the model at a fixed orientation relative to the guideway. The data from these tests indicate some aerodynamic interference between the carriage and the flow over the upper surface of the model.

Simplified theories are developed for the flow over the upper surface of the model and for the effect of pitch attitude on the flow under the lower surface. The level of agreement between the theory and the various testing techniques is discussed.

17. Key Words	18. Distribution Statement
Ground Effect Ram Wind Ram Air Cushion Tracked Levitated Vehicle High-Speed Ground Transportation	DOCUMENT IS AVAILABLE TO THE PUBLIC THROUGH THE NATIONAL TECHNICAL INFORMATION SERVICE, SPRINGFIELD, VIRGINIA 22161

19. Security Classif. (of this report)	20. Security Classif. (of this page)	21. No. of Pages	22. Price
UNCLASSIFIED	UNCLASSIFIED	142	

Form DOT F 1700.7 (8-72) Reproduction of completed page authorized

PREFACE

Research into the possibility of using aerodynamic lift for application to ground transportation vehicles has been carried out at a very low level for approximately 12 years. This has been limited to simple analytical investigations and small-scale experiments. During this time, the concept has gone through considerable evolution beginning with a simple body designed to travel through a tube and reaching the stage of a vehicle traveling in an open guideway with flexibly mounted winglets.

In 1973, a system definition study was completed which described the characteristics of a full-scale system. The so-called Tracked Ram Air Cushion Vehicle (TRACV) requires relatively little energy for suspension and has a potential for low guideway cost due to the large average air gap.

This report is the third in a series describing research conducted at Princeton University on the TRACV. The first report focused on establishing the variation of lift and pitching moment with vehicle height. A later report contains an analysis of vehicles motions over a guideway with random irregularities. The present report focuses on lift and pitching moment variations with pitch attitude.

Funding for this research was provided through the Transportation Advanced Research Program (TARP). This program was originally a part of the Office of the Secretary (OST) but has been transferred to the newly formed Research and Special Programs Administration (RSPA). Technical direction for the effort was provided by the Advanced Systems Office of the Transportation Systems Center.

TABLE OF CONTENTS

LIST OF ILLUSTRATIONS (Cont'd)

LIST OF TABLES

NOMENCLATURE

a_n	equation (3-17)
A	equation (3-41)
$\bar{A}$	ratio of local area to exit area, $\bar{A} = \frac{A_L}{A_E}$
A_E	area between vehicle and guideway at the vehicle trailing edge, ft^2
A_L	area between vehicle and guideway at any chordwise location, ft^2, $A_L(c) = A_E$
A_n	equation (3-17)
A_{SE}	area between sides of vehicle and guideway at the model trailing edge, $A_{SE} = 7.25$ $in.^2$
AR	aspect ratio, $\frac{W}{c}$
b_m	equation (3-20)
c	length of chord of vehicle, ft or in. (c= 72 in.)
C_D	drag coefficient, $C_D = \frac{D}{\frac{1}{2} \rho V^2 S}$
C_H	hinge moment coefficient
C_L	lift coefficient, $C_L = \frac{L}{\frac{1}{2} \rho V^2 S}$
C_M	pitching moment coefficient, referenced to 50 percent chord unless noted by subscript, $C_M = \frac{M}{\frac{1}{2} \rho V^2 Sc}$
C_P	pressure coefficient, $C_P = \frac{p - p_\infty}{\frac{1}{2} \rho V^2}$
D	drag, lb
f	thickness distribution, Figure 14, in Appendix A, $f = \bar{A}\bar{U} - 1$

r_N	r evaluated at $\bar{\alpha} = \bar{\alpha}_N$. $r_N = 0.428$. See Figure C-2
S	vehicle planform area including winglet area ($S = 6.75\ ft^2$), cross section area of ellipsoid
S'	planform area of ellipsoid
U	local velocity, fps
U_E	exit velocity, fps
$\bar{U}$	nondimensional horizontal velocity, $\frac{U}{V}$
V	free-stream velocity, fps
w	velocity at side gap, normal to longitudinal axis of velocity, fps
$\bar{w}$	nondimensional gap velocity, $\frac{w}{V}$
W	width of hull of vehicle, ft or in. (W = 10.875 in.)
$\hat{W}$	body width normalized by semi-chord
W'	weight of vehicle, lb.
x	longitudinal location on model measured from leading edge, ft or in.
$\bar{x}$	nondimensional longitudinal location, $\bar{x} = \frac{x}{c}$
$\bar{x}_{CP,\ LE}$	center-of-pressure location measured from leading edge
x_o	reference axis location from leading edge, ft. ($\bar{x}_o = 0.5$)
α	angle-of-attack of lower surface of vehicle, rad, $\alpha = \alpha_o + \theta$
α_o	angle-of-attack of lower surface of vehicle with winglets parallel to guideway, $\alpha_o = 0.038$ rad.

ξ	dummy integration variable, ft.
ρ	density of air, slugs per ft^3
ϕ	velocity potential
ϕ_G	angle of inclination of guideway lip, rad or deg. (ϕ_G = 45 deg.)
$(\dot{})$	differentiation with respect to time
D	differentiation with respect to non dimensional time, $D(\ ) = \frac{c}{U}\frac{d(\ )}{dt}$

Subscripts

o	defined at reference axis (station x_o)
AX	axisymmetric
c	channel
o	outer
LE	leading edge eigensolution
m	integer index
n	integer index
SE	side exit
TE	trailing edge eigensolution
t	thickness
u	upper
2D	two-dimensional
3D	three-dimensional

Superscripts

i	inner
o	outer

1. INTRODUCTION

This report is concerned with further studies of the aerodynamic characteristics of tracked ram air cushion vehicles (TRACV). Reference 1 presents the results of experimental and theoretical studies of the aerodynamic characteristics of TRACV, concentrating on the influence of vehicle height and winglet gap with respect to the guideway on the lift, drag and pitching moment characteristics. Experimental studies were conducted both in a wind tunnel and with models moving along a guideway using a unique facility at Princeton University. Very good agreement between the aerodynamic forces and moments measured by these two techniques was obtained. In addition, a theory was developed which agreed well with the experimental results especially with respect to the prediction of the stabilty derivatives, that is, the variations in forces and moments about a trim or equilibrium condition.

The aerodynamic measurements indicate that this type of vehicle can achieve quite favorable lift/drag ratios and thus, is attractive as a high speed ground transportation vehicle. In order to fully evaluate the potential of this concept, it is important to be able to quantify its dynamic stability and ride quality. The aerodynamic studies reported here and in Reference 1 are directed towards developing experimentally verified theoretical models for the stability derivatives, such that the dynamic stability and ride qualities of possible full-scale configurations can be estimated in the design stage and such items as the specifications on guideway roughness and possible control systems required in the vehicle to produce good ride qualities can be determined.

2. EXPERIMENTAL PROGRAM

2.1 EXPERIMENTAL APPARATUS AND MODEL

Three distinct sets of experiments were conducted to measure the effect of vehicle pitch attitude on lift, drag and pitching moment. One set was conducted in a wind tunnel. A section of guideway and model were mounted in a wind tunnel and the model lift, drag and pitching moment were measured as a function of vehicle parameters with emphasis on the influence of pitch attitude. The model configuration and dimensions are shown in Figure 1, and Figure 2 shows the model installed in the wind tunnel.

The other two sets of experiments involved the use of an identical model, moved along a 300-foot guideway by a servocontrolled carriage. In one of these sets, the model was essentially in free flight lifting its own weight. The equilibrium position of the model with respect to the guideway was measured as a function of model weight and center-of-gravity position from these equilibrium flight data. For this set of experiments, the model is referred to as the towed-model. The test configuration is shown in Figure 3, and Figure 4 shows the model installed in the test facility, the Princeton Dynamic Model Track. Figure 5 shows the displacement measuring system used to measure the side gap at each of the four corners of the model. The height and attitude of the model can be calculated from these four measurements.

The second set in this series involved the use of the same model. However, the model was mounted on a strain gage balance on a specially designed idler carriage as shown in Figures 6 and 7. For this test

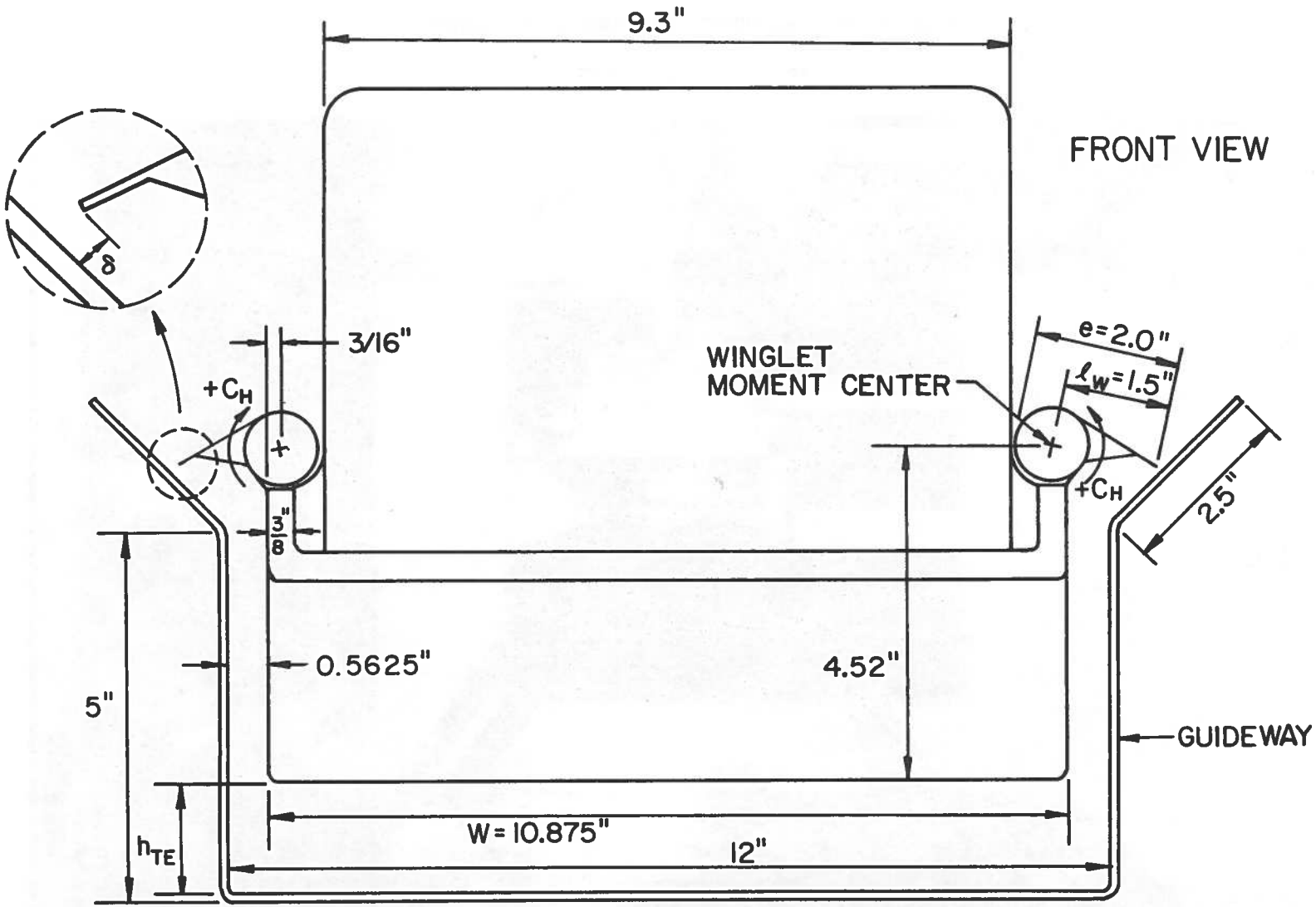

FIGURE 1. WIND TUNNEL MODEL CONFIGURATION (CONTINUED)

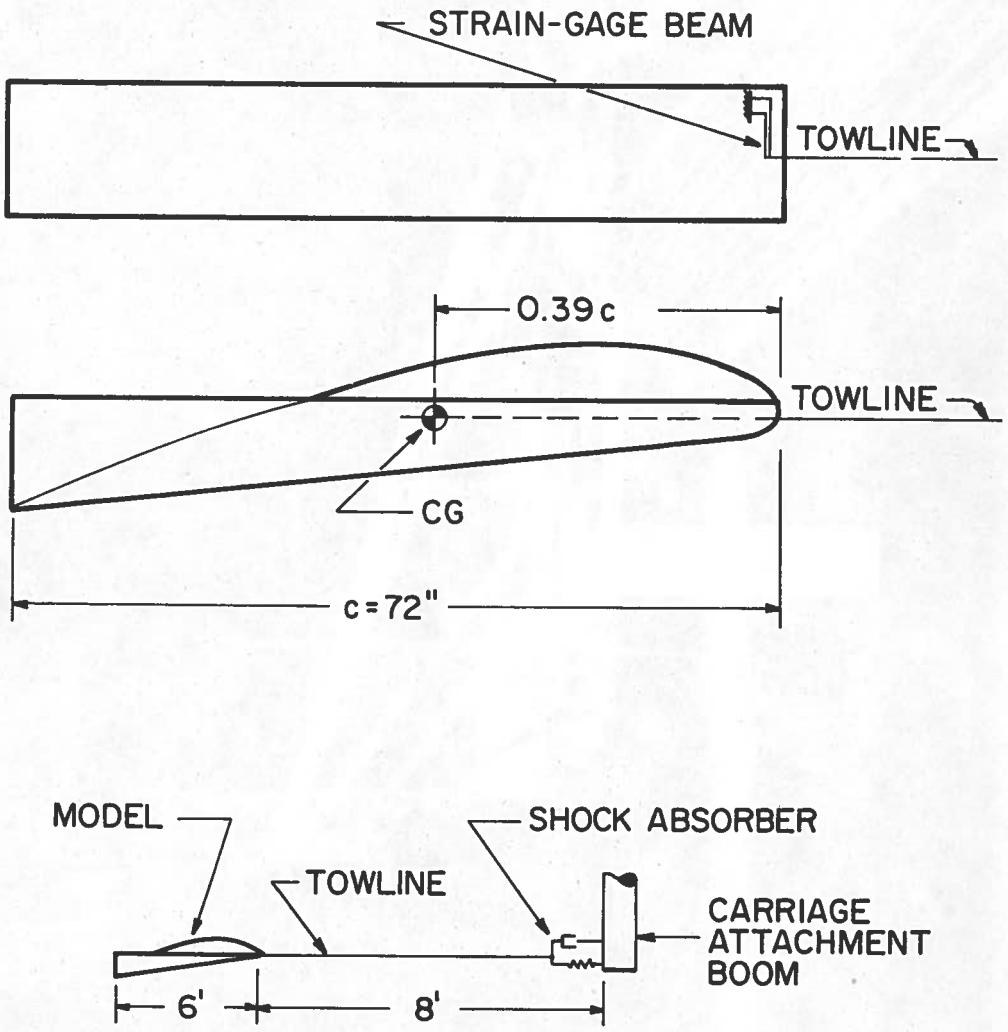

FIGURE 3. TOWED MODEL CONFIGURATION

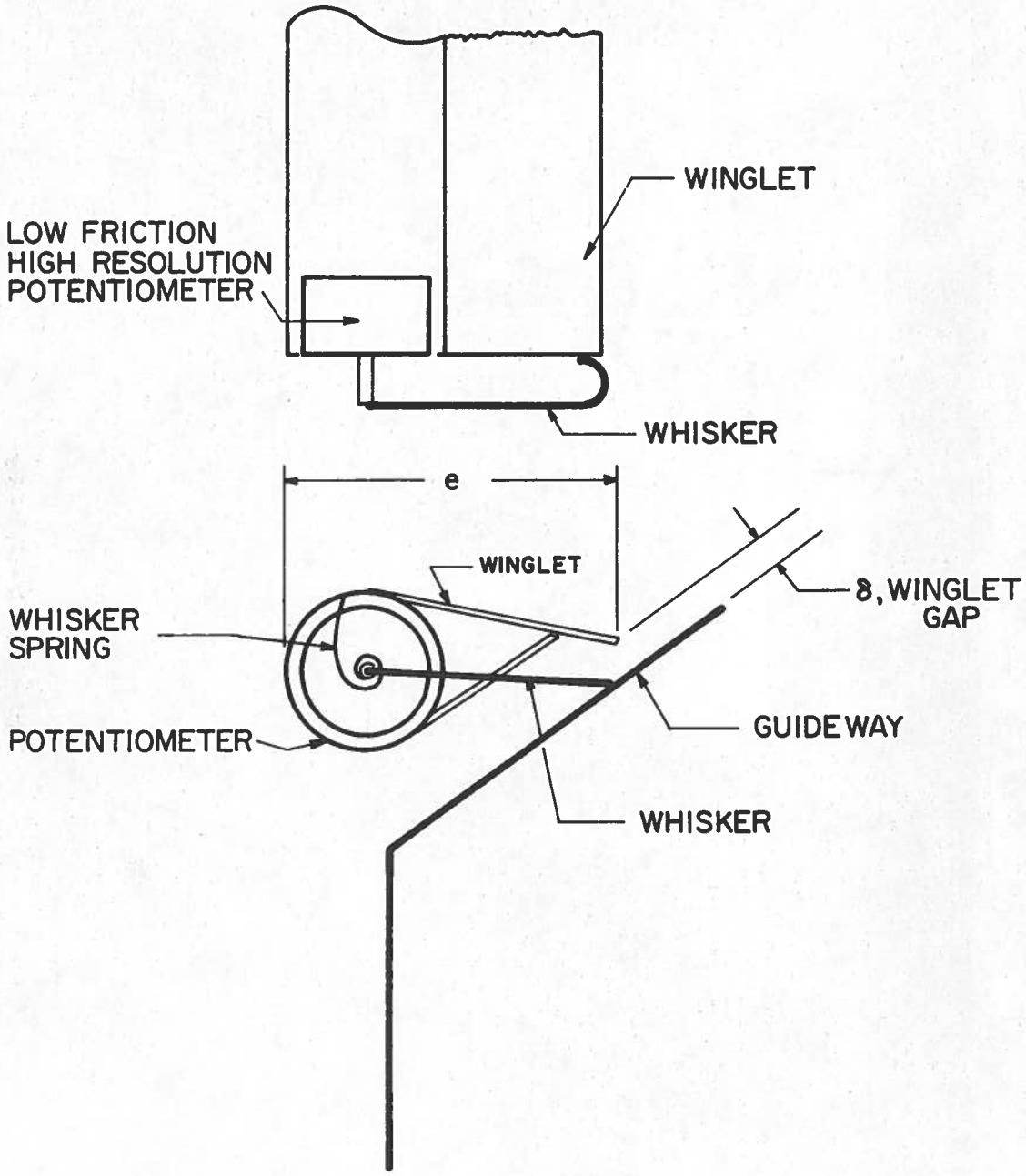

FIGURE 5. DISPLACEMENT MEASURING SYSTEM, TOWED MODEL

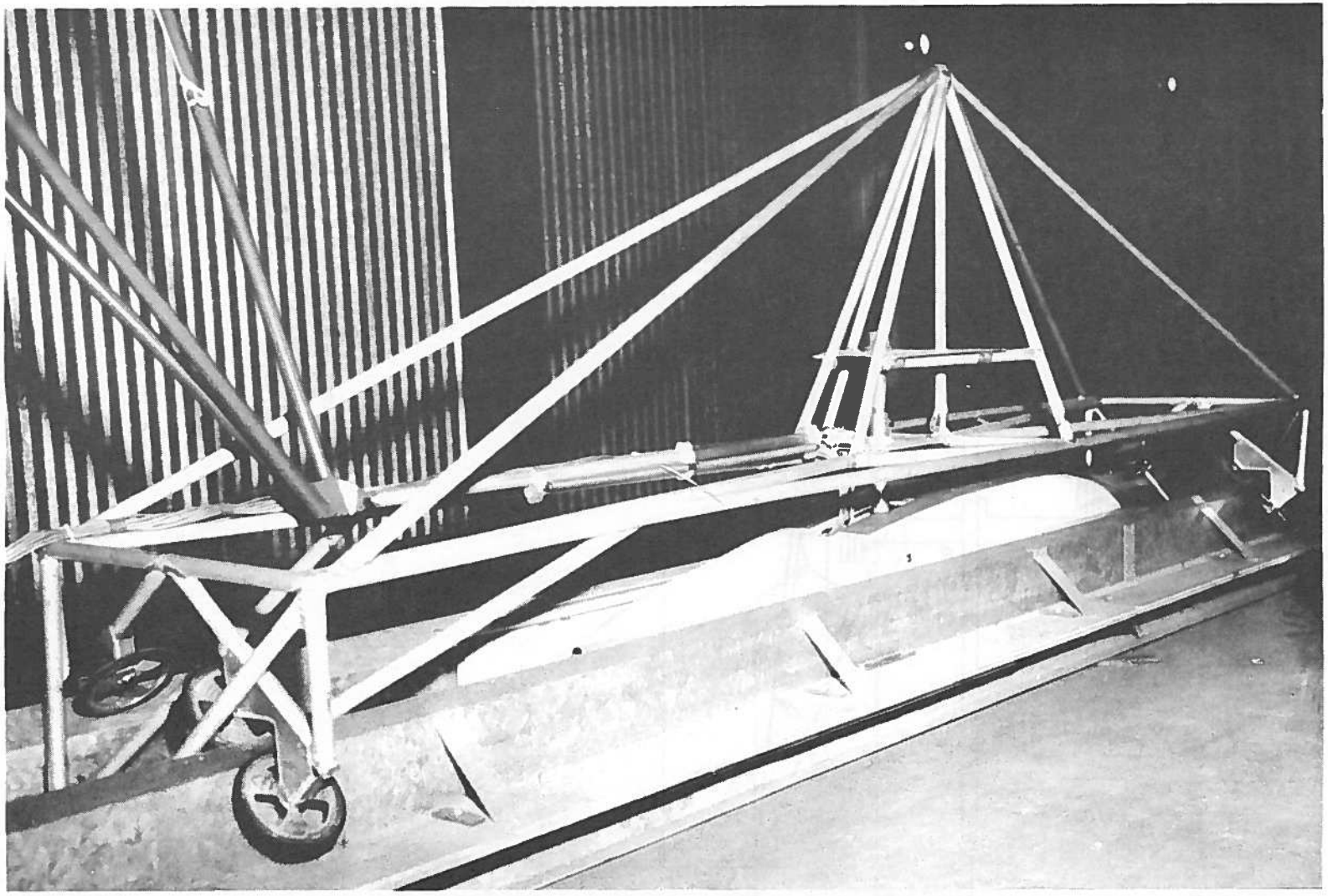

FIGURE 7. CLOSE-UP OF MOVING MODEL AND IDLER CARRIAGE

series, the model is referred to as the moving-model. The idler carriage rides on the guideway on large diameter wheels which can be seen in Figure 7. The large amount of structure above the model was required by the design requirement to provide the rigidity necessary to maintain close tolerances between the model and the guideway.

Each testing technique has its advantages and disadvantages. The wind tunnel tests suffer from the disadvantage that there is a boundary layer present on the guideway which does not exist in the flight of the vehicle. However, Reference 1 shows good agreement between experimental results obtained from these two techniques, indicating that the presence of the boundary layer does not have an important influence on the lift and pitching moment. Wind tunnel experiments tend to be more convenient with regard to studying large numbers of model parameter variations. Experience with wind tunnel testing showed this to be somewhat less true than was originally expected owing to the necessity of careful setting, adjusting and monitoring of the small clearances of the model with respect to the guideway. Higher Reynolds numbers can also be achieved in the wind tunnel.

One advantage of the moving model test in the steady-state case is the elimination of the boundary layer on the guideway. However, as noted above, experimental results presented in Reference 1 indicate that this does not appear to be significant for TRACV. Difficulties were also experienced in the moving-model tests with model guideway contact. This was a result of the fact that to reduce the cost of

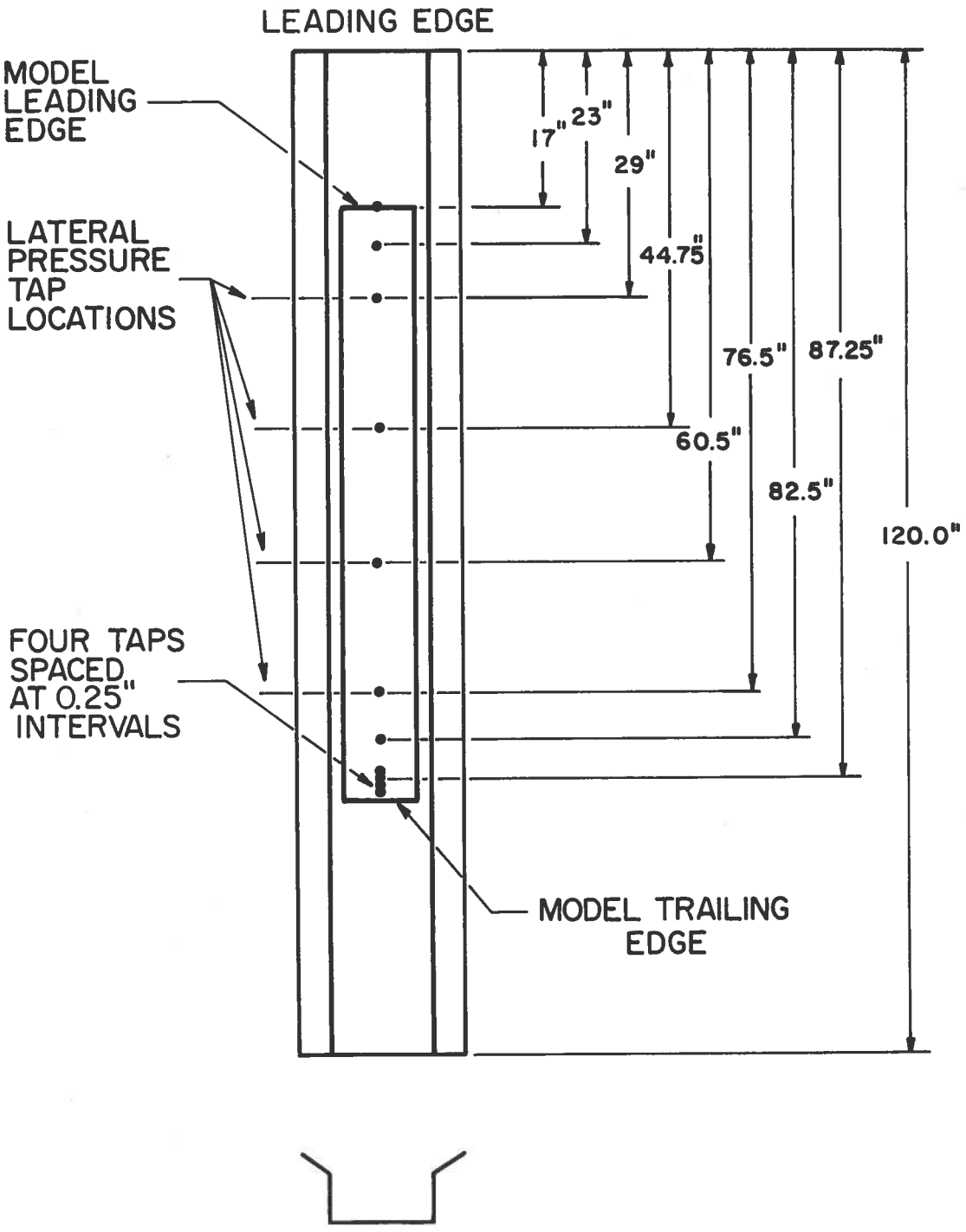

FIGURE 9. GUIDEWAY PRESSURE TAP LOCATIONS, WIND TUNNEL

test conditions and, in general, all three dimensionless variables change when the attitude of the model is changed. All wind tunnel data are presented at a dynamic pressure of 10.4 psf.

The towed model and moving model tests were conducted in the Princeton Dynamic Model Track with model and guideway geometry identical to the wind tunnel tests. The tests were conducted at a nominal model velocity of 34 fps. For the towed-model experiments, weights were added to the model to vary its gross weight and center-of-gravity position and the variations in the equilibrium condition of the model with respect to the guideway were measured. From these measurements the stability derivatives of the vehicle can be determined as described in Appendix C, taken from Reference 1. The moving model test involved adjusting the pitch attitude and height of the model for each run. All six forces and moments were measured during the course of a run. Continuous time histories of the forces and moments were recorded and about 10 seconds of data at a steady-state condition were available for analysis. The noise levels in the force and moment data, which arise due to small acceleration inputs from small irregularities in the guideway were maintained at a very low level by employing a light-weight model, such that, the aerodynamic lifting force was comparable to the weight of the model. A typical time history obtained for one run is shown in Figure 10. Only the lift, drag and pitching moment are shown.

For further details of the wind tunnel and towed model tests the reader is referred to Reference 1.

2.2 WIND TUNNEL DATA

2.2.1 Force and Moment Data

The lift coefficient, drag coefficient, and pitching moment coefficient were measured as a function of the dimensionless parameters r_o, r_1, and $\bar{\alpha}$. The term r_o is a dimensionless measure of the winglet gap; r_1 is a dimensionless measure of the vehicle attitude or gap variation along the length of the model and $\bar{\alpha}$ is a dimensionless measure of the height of the trailing edge of the vehicle above the guideway. The primary interest in these experiments was the determination of the influence of r_1. However, recalling the definitions of the three parameters, for $\bar{x}_o = 0.5$

$$r_o = \frac{\delta_{LE} + \delta_{TE}}{W\alpha}$$

$$r_1 = \frac{2(\delta_{TE} - \delta_{LE})}{W\alpha} \qquad (2\text{-}1)$$

$$\bar{\alpha} = \frac{Wc\,\alpha}{A_E} \; .$$

Since the geometry of the model is fixed, these parameters are interrelated and cannot be set independently. The attitude of the model and the trailing edge height are adjusted at the model support point. The gap at the reference point is adjusted by rotating the winglets about their longitudinal axis shown in Figure 1. The following relationships exist between the adjustable quantities, θ, h_{TE}, and δ_o and the dimensionless quantities appearing above.

comparison between theory and experiment is reasonably good over the forward forty percent of the body. The theory overestimates the pressure on the after end of the body and the experimental data show a small suction at the trailing edge. It is possible that correlation between theory and experiment could be improved by modifying the boundary condition at the trailing edge. The differences between theory and experiment are similar to those found in Reference 1.

2.3 TOWED-MODEL DATA

The results of the towed model experiments are shown in Figure 14 in terms of the slopes of the lift coefficient and pitching moment coefficient with pitch attitude as a function of the dimensionless equilibrium flight gap and the nominal value $\bar{\alpha}_N$. The value of $\bar{\alpha}$ corresponding to $\bar{\alpha}_N$ is given by the relationship

$$\bar{\alpha} = \frac{\bar{\alpha}_N}{1 + \frac{1}{2} \frac{\bar{\alpha}_N}{\cos \phi_G} \frac{W}{c} (r_o - 0.428)} \quad . \tag{2-3}$$

Appendix C, from Reference 1, describes how these stability derivatives were determined from the experimental measurements. The experimental data from which these results were calculated is presented in Reference 1.

The attitude derivatives, that is, the variation of lift coefficient and pitching moment with pitch attitude, with height constant, about an equilibrium or trim condition, are found from measurements of the model displacement with respect to the guideway as a function of model loading condition.

The experimental results shown in Figure 14 indicate that the variation of lift coefficient with attitude increases as the dimensionless

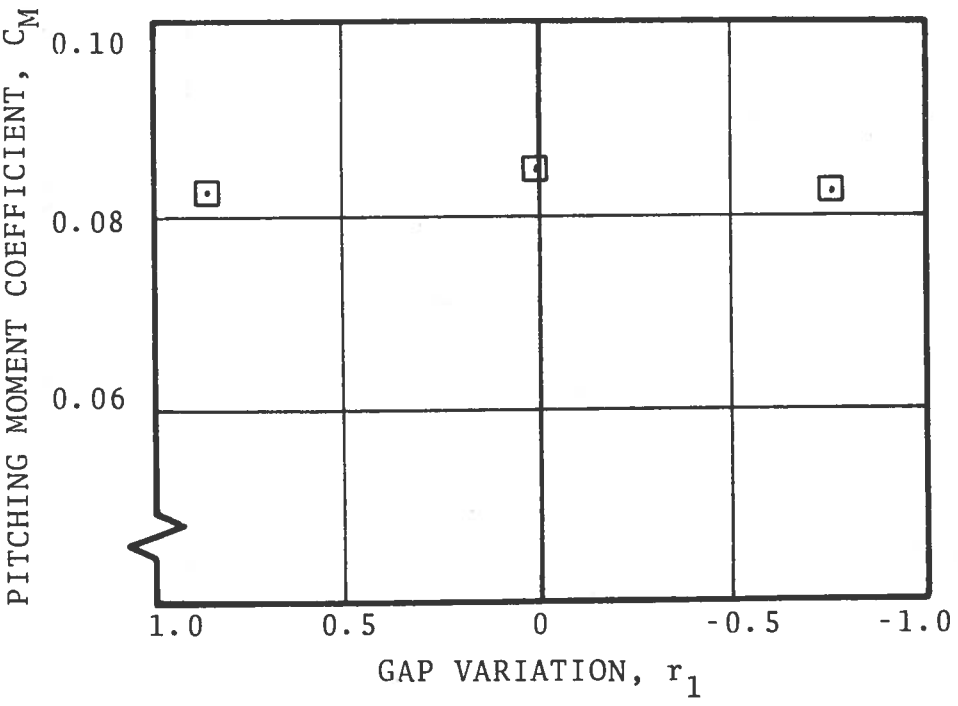

FIGURE 11. WIND TUNNEL DATA (CONTINUED)

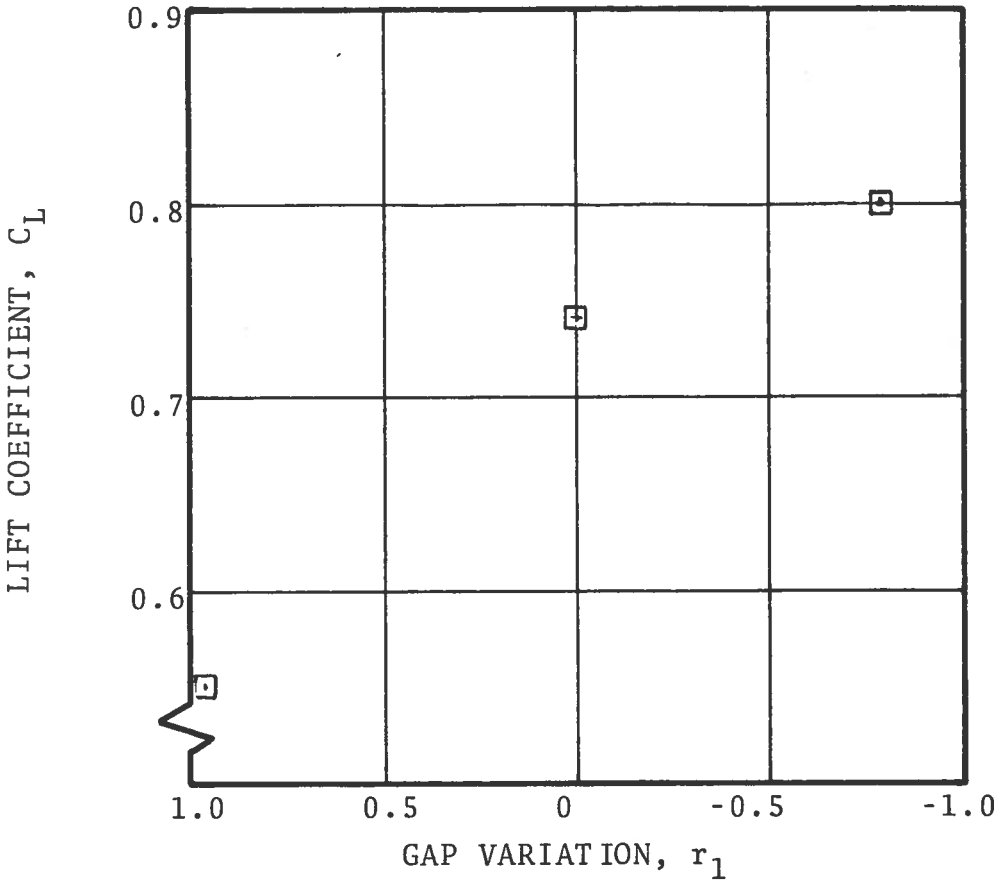

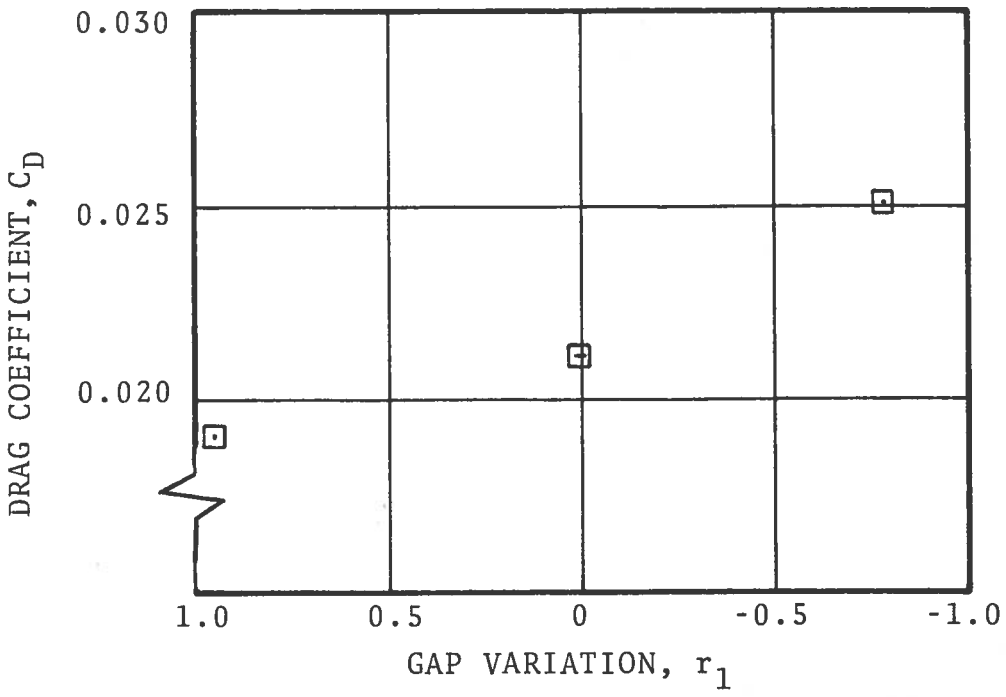

FIGURE 12. WIND TUNNEL DATA ($\bar{\alpha}$ = 1.36, r_0 = 0.54 at r_1 = 0)

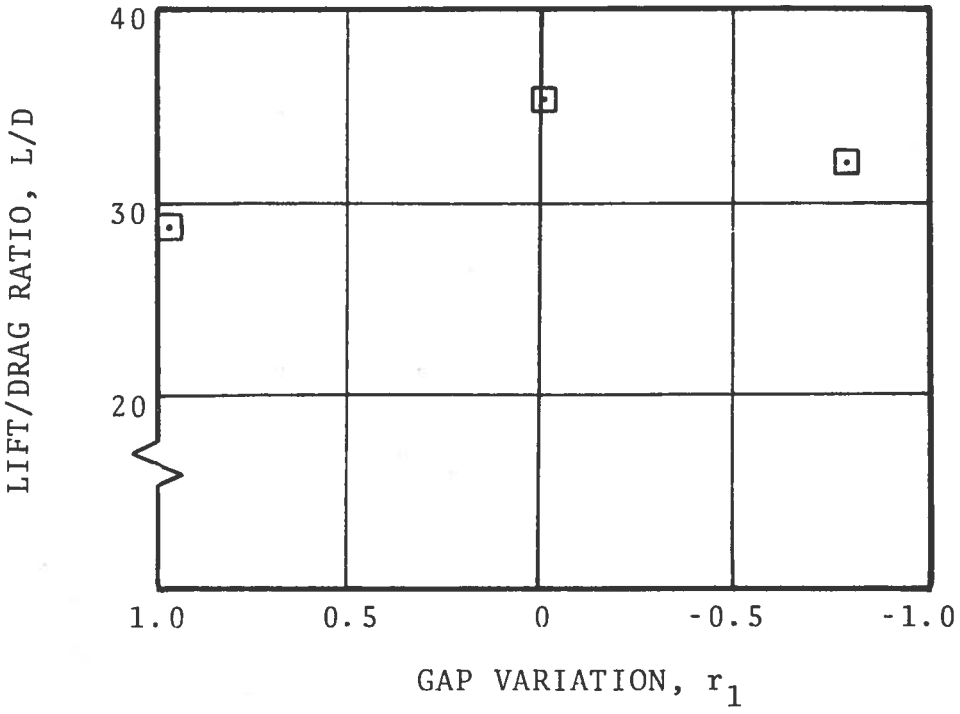

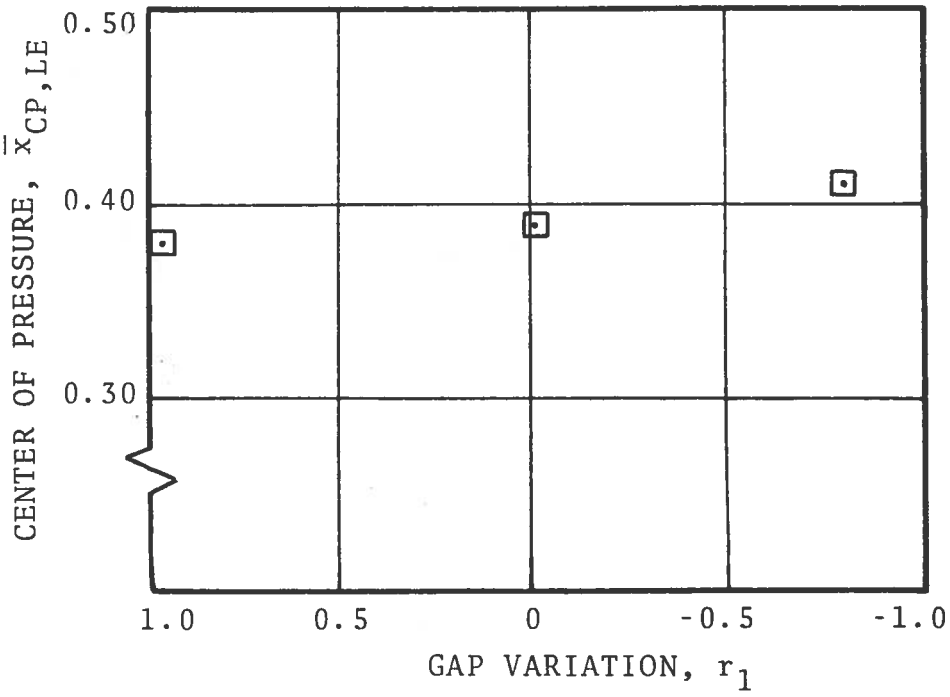

FIGURE 12. WIND TUNNEL DATA (CONTINUED)

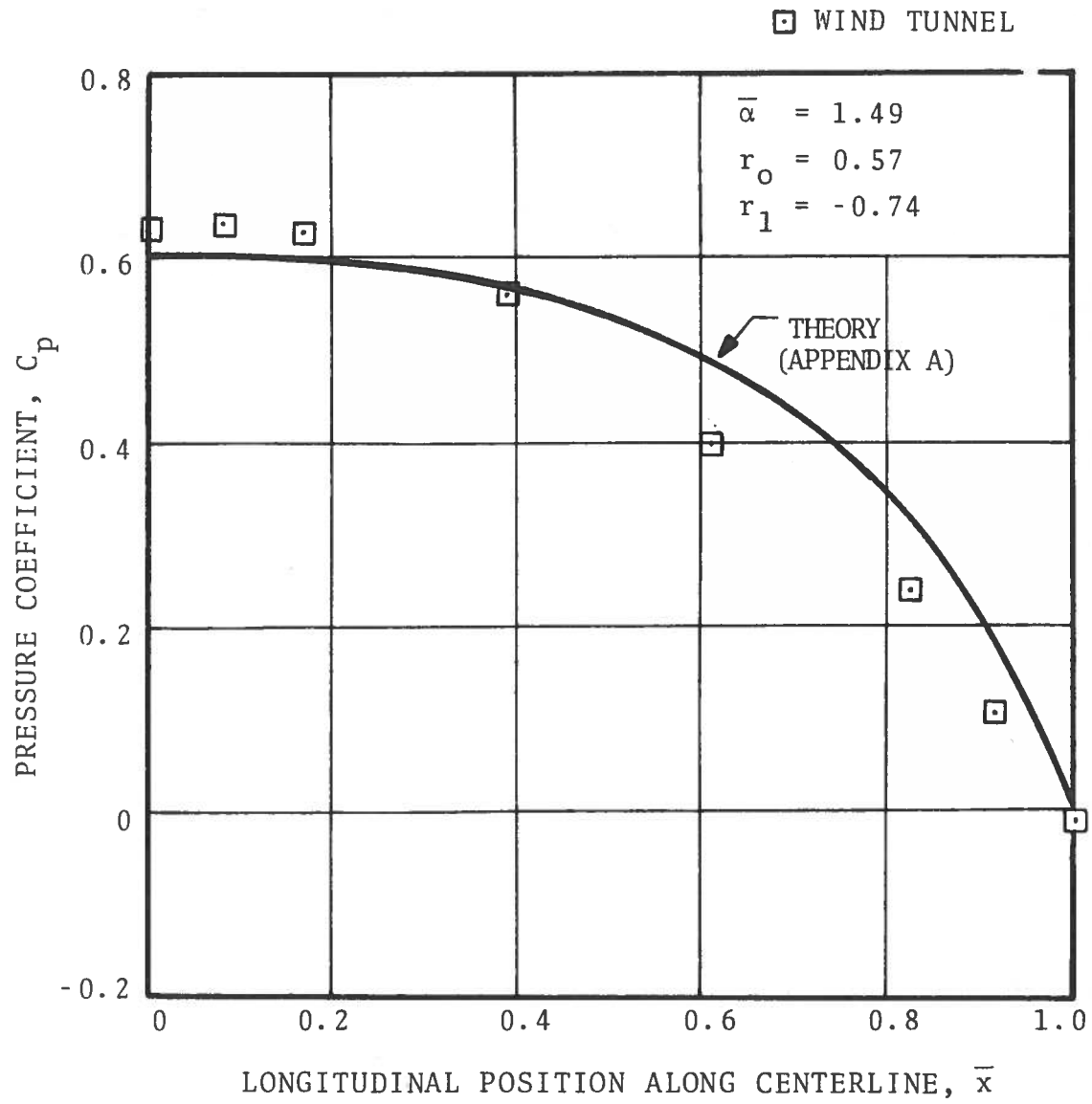

FIGURE 13. LOWER SURFACE PRESSURE DISTRIBUTION, WIND TUNNEL (CONTINUED)

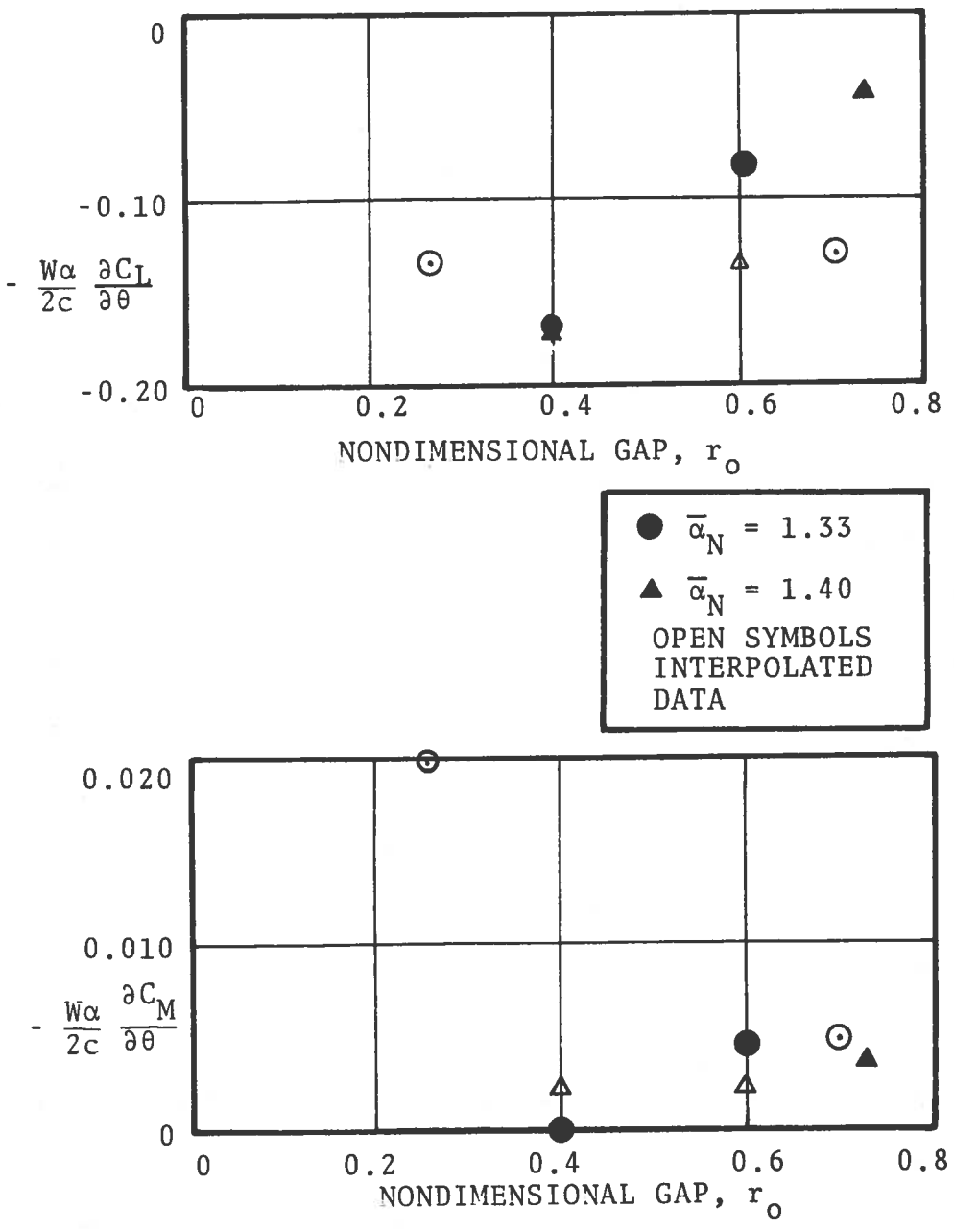

FIGURE 14. TOWED MODEL DATA

TABLE 2. MOVING MODEL TEST CONDITIONS (IDLER CARRIAGE)

CASE	h_{TE} in	$\delta_{.167}$ in	δ_{TE} in	δ_0 in	δ_1 in	θ rad	α deg	$\bar{\alpha}$	r_0	r_1
A-L	1.31	0.11	0.11	0.11	0	0	2.16°	1.37	0.54	0
A-U	1.18	0.185	0.018	0.118	-0.201	0.0039	2.38°	1.62	0.52	-0.89
A-D	1.54	0.080	0.27	0.156	0.228	0.0045	1.90°	1.08	0.86	1.26
B-L	1.09	0.10	0.10	0.10	0	0	2.16°	1.54	0.49	0
B-U	1.00	0.095	0.038	0.072	-0.069	0.0014	2.24°	1.68	0.34	-.32
B-D1	1.22	0.036	0.190	0.098	0.185	-0.0036	1.95°	1.30	0.53	1.00
B-D2	1.19	0.055	0.165	0.099	0.132	-0.0026	2.01°	1.36	0.52	0.69

L = Level $A_E = 7.25 + 10.88\ h_{TE}$

U = Nose up $c = 72$ in

D = Nose Down $W = 10.88$ in

$$\theta = \frac{-\delta_1}{c \cos \phi_G} \qquad r_0 = \frac{2\delta_0}{W\alpha} \qquad \delta_0 = \delta_{TE} + 0.6\ (\delta_{.167} - \delta_{TE})$$

$$\bar{\alpha} = \frac{wc\alpha}{A_E} \qquad r_1 = \frac{2\delta_1}{w\alpha} \qquad \delta_1 = \frac{6}{5}\ (\delta_{TE} - \delta_{.167})$$

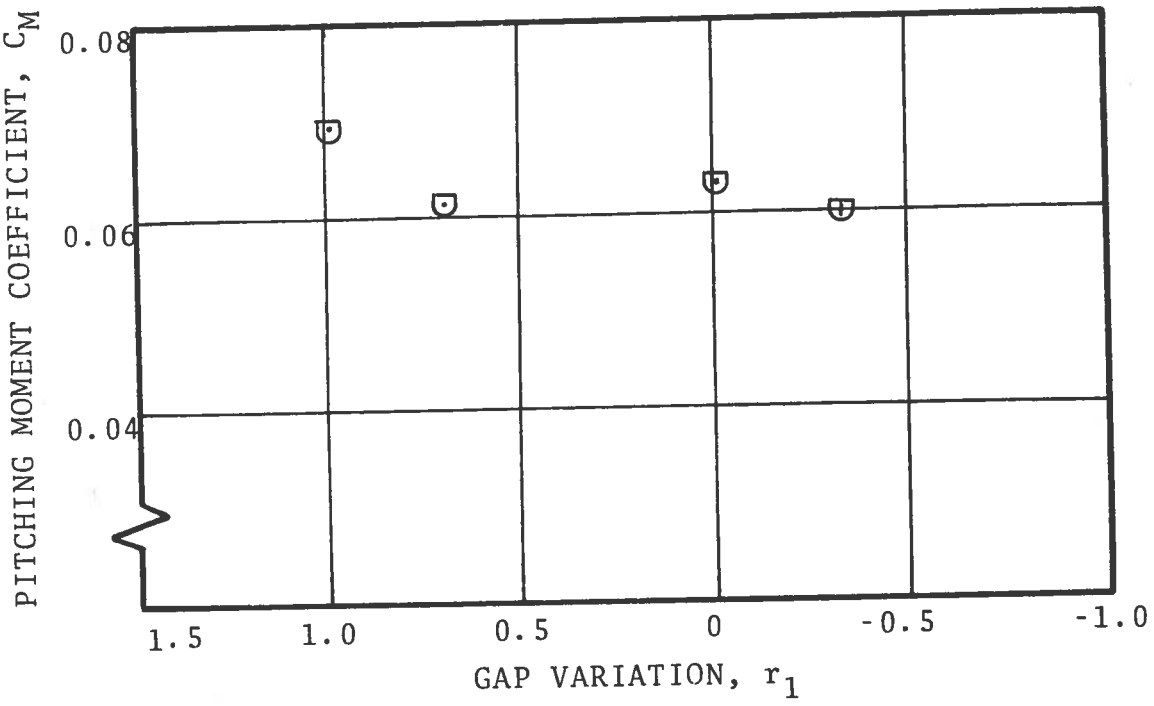

FIGURE 15. MOVING-MODEL DATA (CONTINUED)

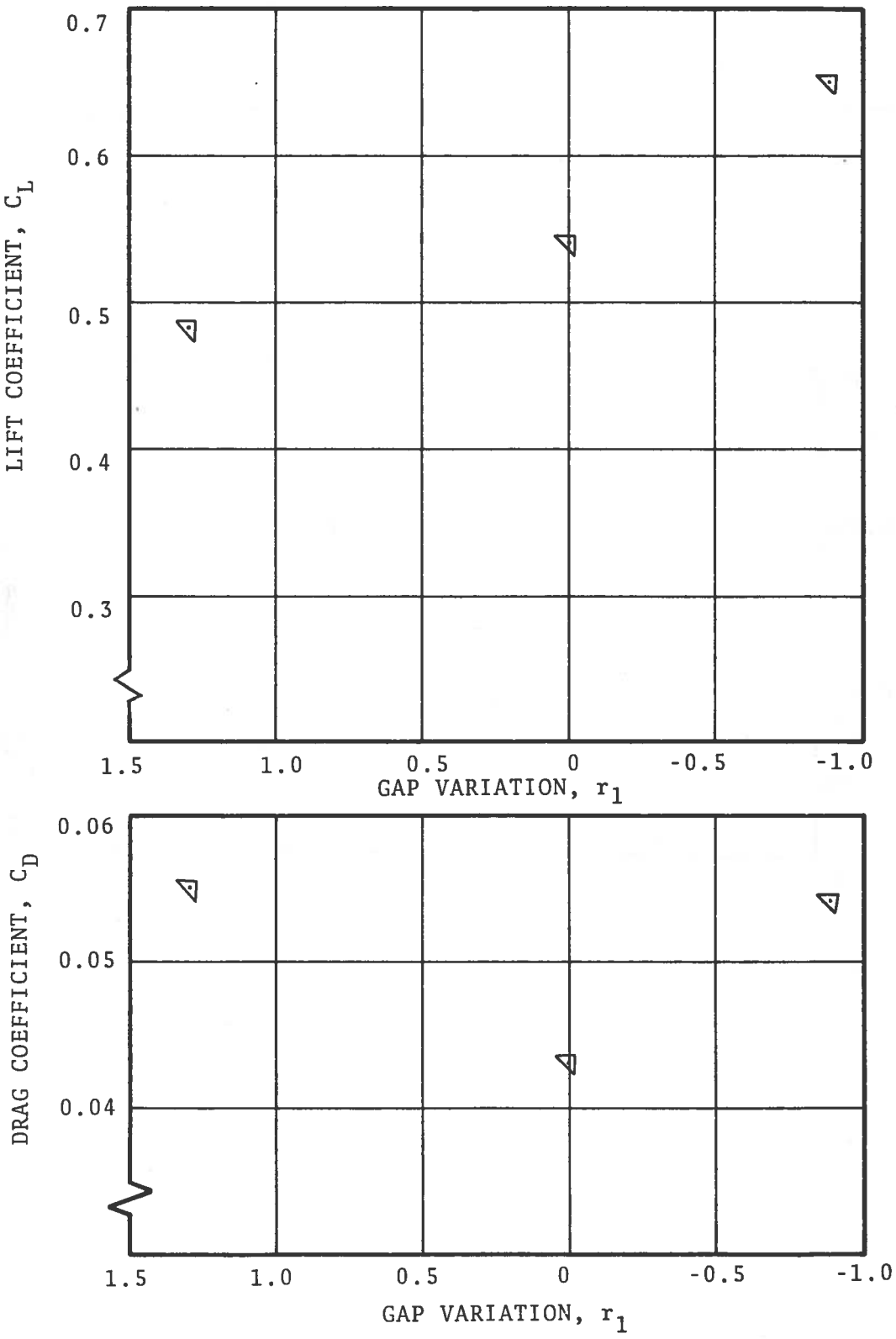

FIGURE 16. MOVING MODEL DATA ($\bar{\alpha}$ = 1.37, r_o = 0.54, at r_1 = 0)

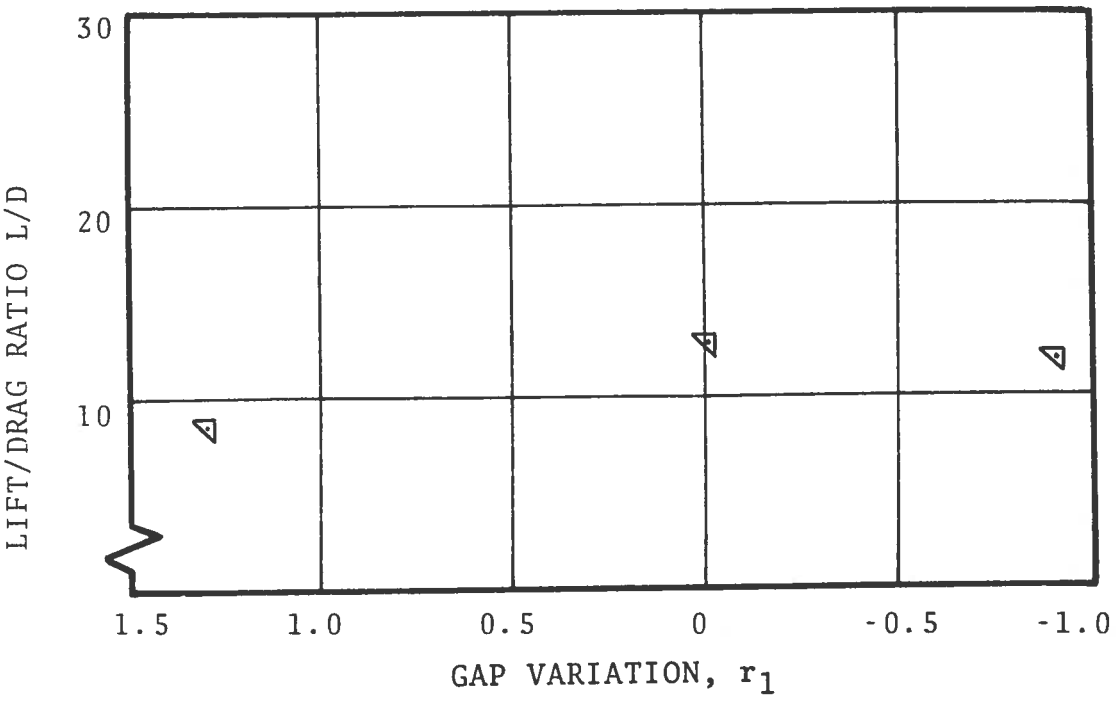

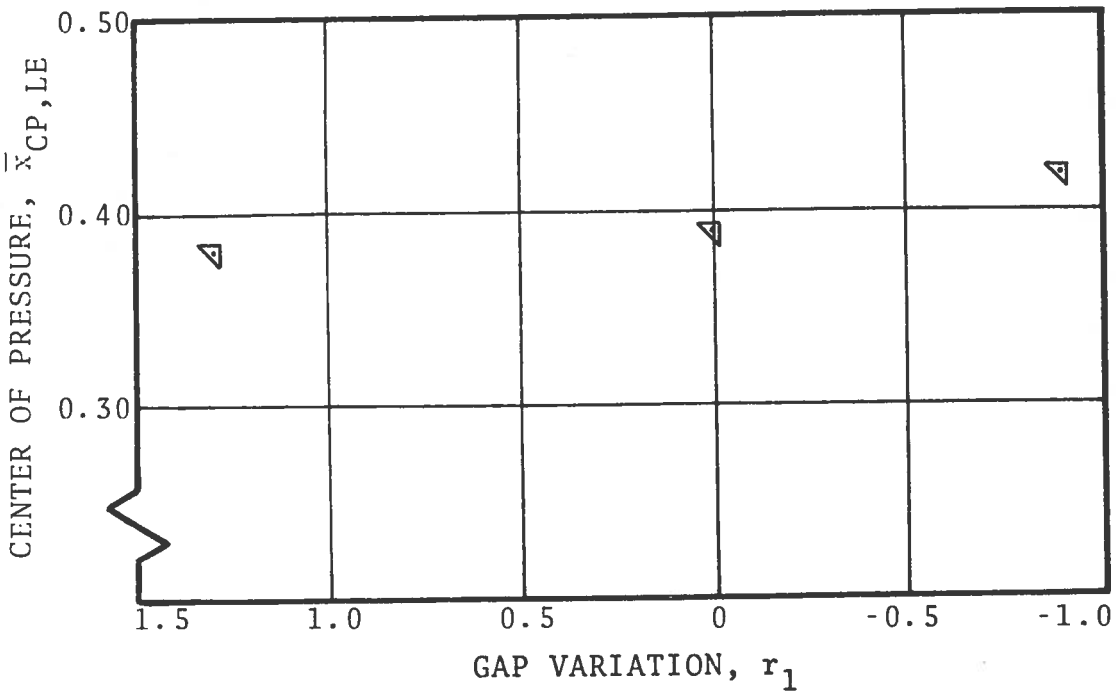

FIGURE 16. MOVING-MODEL DATA (CONTINUED)

3. UPPER SURFACE THEORY

In Reference 1, rough approximations were used to estimate the contribution of the upper surface of the TRACV. This section presents a more refined analysis of these contributions.

The central idea behind the analysis of a wing-in-ground effect is that the flow can be separated into a channel flow under the wing and a flow over the top of the wing referred to as the outer flow. The channel flow is considered in Appendix A. The outer flow for the case of a two-dimensional flat plate has been analyzed by Barrows, Widnall, and Richardson[2], who showed how the channel flow and the outer flow could be matched using asymptotic expansions. In this section the effect of a thickness distribution on the outer flow is analyzed. It is maintained that this problem can also be analyzed using superposition, that is, the outer flow pressure distribution is the sum of effects due to angle of attack and those due to thickness. The resultant lift must be added to the channel flow effect in order to obtain the total lift. All of the effect of the vertical gap appears in the channel flow, and the outer flow may be analyzed as if this gap were nonexistent. Thus, by using the method of images, the two-dimensional thickness problem reduces to the flow past a symmetrical airfoil, which has been analyzed extensively in the literature. The model shape used in the present experiments is one half of an NACA 0021 airfoil, for which a pressure distribution, calculated using Theodorsen's methods, is given by Abott and von Doenhoff[3]. Lee[4] has used this distribution to calculate the outer flow lift and pitching moment for the experimental model. Even though this is a worthwhile and logical calculation, there remain two major deficiencies with this approach:

$$C_L = 2 \Gamma \alpha \tag{3-1}$$

$$\Gamma = \Gamma_c + \Gamma_{LE} + \Gamma_{TE} + \Gamma_o \tag{3-2}$$

where

α = angle of attack

Γ_c = channel flow circulation

Γ_{LE} = leading edge circulation

Γ_{TE} = trailing edge circulation

Γ_o = outer flow circulation.

The most important term, Γ_c, may be calculated using one-dimensional channel flow which may easily be extended to include the effect of leakage at the side edges using the method of Barrows[5] or Curtiss and Putman.[1] The trailing edge contribution is mainly due to the fact that the pressure at the trailing edge is somewhat higher than ambient pressure, rather than equal to ambient as is assumed during the calculation of Γ_c. For purely two-dimensional flow this elevated pressure is felt under the entire under surface of the wing. However, with leakage at the side edges this elevated pressure becomes a local phenomena with very little effect on the total lift. Wind tunnel data[1] show that the channel flow pressures are reasonably close to theoretical predictions which ignore Γ_{TE}, except for points located near the trailing edge. For this reason Γ_{TE} is henceforth neglected.

For a flat plate Γ_o turns out to be $1/\pi$. The angle of attack α is necessarily quite small for a ram wing; specifically, it is 0.038 radians for the wind tunnel model, giving a contribution to the lift of $C_{L_o} = 0.0242$. (The actual contribution is smaller due to the three-dimensional effects.)

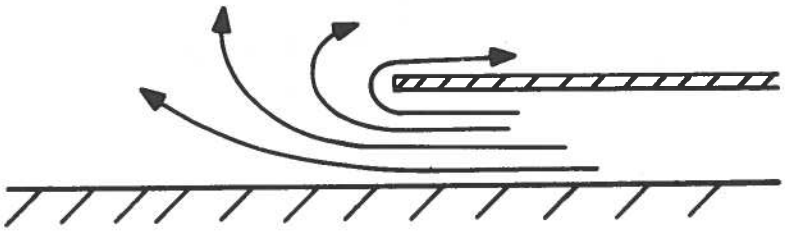

FIGURE 17. MAGNIFIED VIEW OF THE FLOW AT THE LEADING EDGE OF A FLAT PLATE IN GROUND PROXIMITY, WITH THE FREESTREAM COMPONENT SUBTRACTED

Reference 2 gives the following for the leading edge contribution for the flat plate:

$$\Gamma_{TE} = \frac{1}{\pi} \ln \frac{\pi}{\varepsilon}, \tag{3-3}$$

where ε is the leading edge clearance normalized by the chord. With the trailing edge touching, $\alpha = \varepsilon$, which may be inserted into equation (3-1) to obtain

$$C_{L_{LE}} = \frac{2\varepsilon}{\pi} \ln \frac{\pi}{\varepsilon} . \tag{3-4}$$

Turning now to the wedge, when we magnify the x coordinate we obtain the flow past a step, Figure 19, which can be analyzed using a Schwarz-Christoffel transformation as shown by Milne-Thompson.[6] The solution for the surface speed q appears in terms of a parameter ζ as follows:

$$q = V\sqrt{\frac{\zeta + 1}{\zeta - 1}} \tag{3-5}$$

where

$$\bar{x} = \frac{\varepsilon}{\pi} \left(\sqrt{\zeta^2 - 1} - \cosh^{-1} \zeta\right) . \tag{3-6}$$

and the coordinate system is located such that the step occurs at $x = 0$. The lift coefficient is computed as follows:

$$C_L = \int_0^1 \left[\frac{q^2}{V^2} - 1\right] d\bar{x} \tag{3-7}$$

$$= \int_1^{\zeta_1} \left[\frac{\zeta + 1}{\zeta - 1} - 1\right] \frac{d\bar{x}}{d\zeta} \, d\zeta \tag{3-8}$$

where ζ_1 is the value of ζ corresponding to $\bar{x} = 1$. Differentiating (3-6), we obtain

$$\frac{d\bar{x}}{d\zeta} = \frac{\varepsilon}{\pi}\sqrt{\frac{\zeta - 1}{\zeta + 1}} .$$

$$C_{L_{LE}} = \frac{2\alpha}{\pi} \ln \frac{\pi}{\epsilon} \tag{3-11}$$

where

$$\epsilon = h_{LE}/c \tag{3-12}$$

$$\alpha = (h_{LE} - h_{TE})/c \tag{3-13}$$

h_{LE} = Leading edge height

h_{TE} = Trailing edge height .

Since the leading edge is not generally sharp, some judgement may be required as to the best value of h_{LE}. Whatever value is selected must be consistent with the definition of the thickness distribution of the airfoil, which is discussed in the next section.

3.2 LIFT DUE TO A TWO-DIMENSIONAL THICKNESS DISTRIBUTION

As mentioned above, this type of problem can and has been solved using Theodorsen's method to calculate the surface pressures on the upper half of the NACA 0021 airfoil used in the experiments. The purpose of this section is to point out that much simpler methods exist for predicting the lift and moment, methods which are more readily extended to three dimensions.

Thin wing theory[7] gives the following for the velocity potential on a symmetrical thickness distribution (as shown in Figure 20):

$$\phi(\bar{x}) = \frac{1}{\pi} \int_0^1 f'(\bar{x}_1) \ln (\bar{x} - \bar{x}_1) \, d\bar{x}_1 \tag{3-14}$$

where

f = thickness distribution function

and

$f' = df/d\bar{x}$.

The lift coefficient due to thickness C_{L_t} may be found from

$$C_{L_t} = \int_o^1 C_p \, d\bar{x} = -2 \int_o^1 \frac{d\phi}{d\bar{x}} \, d\bar{x} = 2\phi\,(0) - 2\phi\,(1). \qquad (3\text{-}15)$$

Thus,

$$C_{L_t} = \frac{2}{\pi} \int_o^1 f'(\bar{x}_1) \left[\ln \bar{x}_1 - \ln (1 - \bar{x}_1)\right] d\bar{x}_1 \quad .$$

This may be integrated by parts:

$$C_{L_t} = \frac{2}{\pi} \left[f(\bar{x}) \ln (\bar{x}) - f(\bar{x}) \ln (1 - \bar{x})\right]_o^1 + \frac{2}{\pi} \int_o^1 \frac{f(\bar{x})\, d\bar{x}}{\bar{x}\,(1 - \bar{x})}$$

The first term above disappears since $f(0) = f(1) = 0$.

Thus,

$$C_{L_t} = \frac{2}{\pi} \int_o^1 \frac{f(\bar{x})\, d\bar{x}}{\bar{x}\,(1 - \bar{x})} \quad . \qquad (3\text{-}16)$$

The NACA 00XX series airfoils are given as follows:

$$f = \frac{t}{2} \left(A_o \bar{x}^{1/2} + A_1 \bar{x} + a_2 \bar{x}^2 + a_3 \bar{x}^2 + a_4 \bar{x}^4\right) \qquad (3\text{-}17)$$

where

$$A_o = +\,2.969$$

$$A_1 = -\,1.260$$

$$a_2 = -\,3.516$$

$$a_3 = +\,2.843$$

$$a_4 = -\,1.015 \quad .$$

This value is somewhat higher than the value of 0.32 which was obtained by Lee.[4] The reason for this is that thin wing theory is dependent on the assumption that the velocity perturbations are everywhere small compared with the freestream velocity. This is valid everywhere except near a stagnation point. Van Dyke[8] has given an explanation of how to correct thin wing theory for such nonuniformities in the solution, using matched asymptotic expansions. The stagnation point at a sharp trailing edge gives rise to a very weak singularity which may safely be ignored. However, a round leading edge has a larger stagnation region which gives rise to a significant change in the lift. The method of solution is to take a magnified view of the leading edge, which has a parabolic shape. Let us define the new small parameter ε:

$$\varepsilon = \sqrt{2\,r} \tag{3-24}$$

where

r = leading edge radius .

Then the airfoil coordinate near the leading edge may be described by the parabola

$$f = \varepsilon\sqrt{x} \quad . \tag{3-25}$$

Comparison with equation (3-17) shows that

$$\varepsilon = \frac{A_o\, t}{2} \ , \tag{3-26}$$

that is, ε is proportional to the thickness ratio, which is the basic small parameter in thin wing theory. Magnified inner variables are

where C_p^{io} is the outer limit of the inner solution. The basic idea is to add the two solutions together and subtract the common part. In our present case we only need to match to within O(1), for which we obtain

$$C_p^{io} = 0 . \tag{3-31}$$

A "nose correction" ΔC_L to the lift coefficient may be computed as follows:

$$\Delta C_L \equiv - \int_o^1 (C_p^i - C_p^{io})\, dx \quad . \tag{3-32}$$

This is to be added to the outer flow lift as given by equation (3-22). Notice that the integration is taken over the entire surface of the wing, although examination reveals that the major contribution comes from a narrow region near the nose. We obtain, using equation (3-27),

$$\Delta C_L = - \frac{r}{2} \ln \frac{2}{r} \quad . \tag{3-33}$$

For the NACA 0021, r = 0.0485 chords, which gives

$$\Delta C_L = - 0.09 .$$

This may be added to equation (3-23) to obtain

$$C_{L_t} = 0.26 .$$

Now we have a value which is lower than the 0.32 computed by Lee. We could, if desired, improve the accuracy of this result still further by including all of the terms of order ε^2 (which is to say all terms of order t^2) that were thrown out in the first order solution. This exercise would be somewhat involved in comparison to the very simple formulae given here, being borderline between a long hand calculation and a simple computer program. In our present situation, this effort is

given by

$$f(\hat{x}) = t\ (1 - \hat{x})\ (1 + \hat{x}) \tag{3-34}$$

where t is the thickness ratio. The coordinate system is fixed to the center of this airfoil, with the leading and trailing edges at $\hat{x} = \pm 1$. In this coordinate system, equation (3-16) becomes

$$C_{L_{2D}} = \frac{2}{\pi} \int_{-1}^{+1} \frac{f(\hat{x})\ d\hat{x}}{(1 - \hat{x})(1 + \hat{x})} \tag{3-35}$$

where the subscript 2D is interpreted as "two-dimensional". Performing the indicated integration, we have

$$C_{L_{2D}} = \frac{4t}{\pi} \ . \tag{3-36}$$

For the axisymmetric body we must specify an area distribution function $S(\hat{x})$ in place of the thickness function $f(\hat{x})$. Imagine now taking a certain width $\hat{W}$ of the two-dimensional airfoil. In order for both bodies to have the same area distribution, we must have

$$S(\hat{x}) = 2\hat{W}f(\hat{x}), \tag{3-37}$$

where

$$S(\hat{x}) = \pi r^2,$$

and

$$r(\hat{x}) \equiv \text{the radius of the body.}$$

The logical small parameter, ε, for this problem is the maximum radius of the body. Thus,

$$r = \varepsilon\ (1 - \hat{x}^2)^{1/2} \tag{3-38}$$

where

$$\varepsilon = (2\hat{W}t/\pi)^{1/2} \ . \tag{3-39}$$

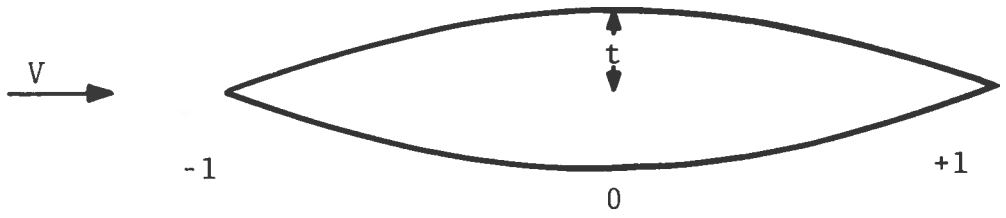

FIGURE 21. BICONVEX AIRFOIL

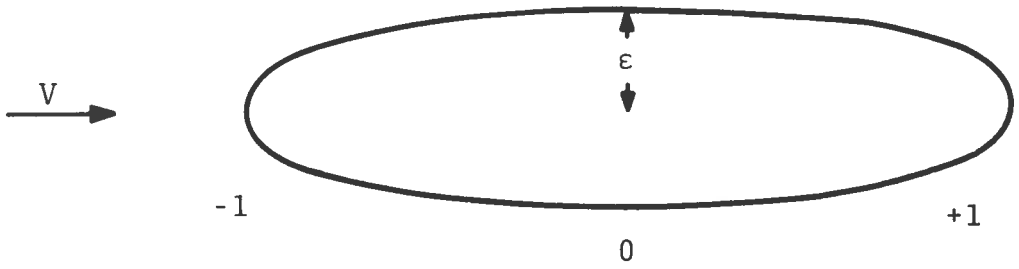

FIGURE 22. ELLIPSOID OF REVOLUTION

$$K = \text{Æ} \left(\ln \frac{\pi}{\text{Æ}\, t} - 3 + 4 \sqrt{\text{Æ}\, t/\pi}\right) . \tag{3-46}$$

For the wind tunnel model we have t = 0.21 and Æ = 1/6. Using these values we obtain

$$K = 0.32, \tag{3-47}$$

that is, a biconvex airfoil of the same thickness ratio as the wind tunnel model would have three times the lift coefficient of the corresponding ellipsoid.

The pressure distributions corresponding to those two bodies are shown in Figure 23. As can be seen, there is some difference in the shape of these distributions, and a considerable difference in the magnitude of the pressure at the center, where the pressure on the airfoil is almost five times that on the ellipsoid.

It seems reasonably safe to assume that the lift on the three-dimensional body defined by taking a certain width W of an airfoil will lie between the limits of two-dimensional flow and axisymmetric flow defined above. As a simple first approach, one might expect the lift to be some kind of average of these two limits. In the lack of any additional information, the geometric mean is as logical as any other average we might define. That is, we hypothesize that

$$C_{L_{3D}} = \sqrt{K}\, C_{L_{2D}} . \tag{3-48}$$

For our present parameters, this makes the lift due to thickness equal to 0.57 times the two-dimensional value. This hypothesis is admittedly crude, but it does give a simple working relationship for the outer flow. One might be tempted to compute a more refined value for K based on the

actual area distribution of the body, but this cannot be done within the confines of slender body theory if the airfoil from which the body is derived has a round leading edge. As mentioned previously, this would result in the equivalent axisymmetric body being too blunt to be represented by a lineal distribution of sources and sinks.

There are some restrictions. This method of approximation is only valid if the thickness ratio and the aspect ratio are comparable and both are << 1. As a matter of coincidence, for the wind tunnel model t turns out to be almost exactly equal to ε, so the equivalent axisymmetric body would have the same maximum thickness, making the method particularly appropriate for this case.

3.4 SUMMARY

In order to calculate the lift on the upper surface, the two-dimensional lift due to thickness is reduced as indicated by equation (3-48) and the lift from the leading edge eigensolution (3-11) is then added:

$$C_{L_u} = C_{L_t} + C_{L_{LE}} \cdot \tag{3-49}$$

A two-dimensional value for the lift coefficient may be readily calculated for thin airfoils using a perturbation expansion. In our present case we may use the value of 0.32 computed by Lee[4], which gives

$$C_{L_u} = 0.18 + 0.10 = 0.28.$$

This value lies below the value determined from the wind tunnel tests (0.30) and that determined from the towed-model tests (0.32) indicated in Reference 1. Comparison with the experimental results of Section 2 is discussed in Section 4. As noted in Section 4, the moving model

Using equation (3-12) for the definition of the leading edge clearance ratio ε, we have

$$\varepsilon = \left(\frac{\alpha}{\bar{\alpha}} - \frac{A_{SE}}{Wc} + \alpha\right) \quad .$$

Applying equation (3-49) to equation (3-11), and using the nominal value of the leading edge height (4.25 in.) we obtain

$$\left(C_{L_{\bar{\alpha}}}\right)_{LE} = \frac{2}{\pi\varepsilon}\left(\frac{\alpha}{\bar{\alpha}}\right)^2 \cong 0.012.$$

This is approximately 10 percent of the theoretical contribution from the channel flow. The wind tunnel results of Reference 1 indicate a value of $C_{L_{\bar{\alpha}}}$ which is twice as great as the theoretical prediction from the channel flow alone, although there is some scatter in the data. Adding the above contribution gives a slight improvement to the agreement between theory and experiment, but not enough to obtain good agreement. The resulting comparison may be termed poor but adequate, since the major contribution to the height stability comes from C_{L_r}.

3.5 EXTENSION OF OUTER FLOW THEORY

If it becomes important to obtain a more accurate model of the outer flow, the approach which is suggested is to represent the body with sources and sinks distributed over the planform of the vehicle as illustrated in Figure 24. A considerable simplification is obtained if the source distribution function f' is constant with y and all the sources are located in the plane $z = 0$. Normalizing all lengths by the semispan of the body, we obtain a formula analogous to equation (3-14):

$$\phi(\hat{x},\hat{y}) = \frac{-1}{2\pi} \int_{o}^{c} \int_{-1}^{+1} \frac{f'(\hat{x}_1)\, d\hat{y}_1\, d\hat{x}_1}{\sqrt{(\hat{x} - \hat{x}_1)^2 + (\hat{y} - \hat{y}_1)^2}} \tag{3-51}$$

where $\hat{x}_1$, $\hat{y}_1$ specifies the location of the source f'. The integration with respect to $\hat{y}_1$ can be carried out directly, and the result is obtained in the form

$$\phi(\hat{x},\hat{y}) = \frac{-1}{2\pi} \int_{o}^{c} k(\hat{x},\hat{y},\hat{x}_1)\, f'(\hat{x}_1)\, d\hat{x}_1 \tag{3-52}$$

where

$$k = \ln \left[\frac{\sqrt{(\hat{x} - \hat{x}_1)^2 + (\hat{y} - 1)^2} + (1 - \hat{y})}{\sqrt{(\hat{x} - \hat{x}_1)^2 + (\hat{y} + 1)^2} - (1 + \hat{y})} \right] \tag{3-53}$$

In general, this integral is too complicated to evaluate analytically. However, with due attention to singularities, it can be evaluated numerically. The singularity may be reduced by integrating by parts:

$$\phi = \frac{1}{2\pi} \int_{o}^{c} f(\hat{x}_1) \frac{dk}{d\hat{x}_1}\, d\hat{x}_1 \quad . \tag{3-54}$$

If this approach is taken, it becomes necessary to correct for the stagnation region at the nose, as illustrated previously.

The results of the analysis so far give a greater understanding of the flow pattern but show only small changes in the overall values of lift and pitching moment. This tends to support the notion that highly refined calculations of the outer flow are not warranted at the present stage of development. Techniques are available to do this for three-dimensional shapes, but a substantial computer programming effort would

4. COMPARISON OF THEORY AND EXPERIMENT

The primary emphasis in the comparison of theory and experiment is aimed towards the evaluation of the simplified theory presented in calculating the stability derivatives of the vehicle. Therefore, only the lift and pitching moment derivatives are discussed since these are largely responsible for the important dynamics associated with the heave motion. It has been shown in Reference 1 that this theory, which is presented in Appendix A, predicts the variation of lift and pitching moment coefficient with height very well, certainly with very satisfactory accuracy for a dynamics and ride quality investigation. Here the interest is centered about the pitch attitude effects, and the adequacy of the extended theory in predicting these effects. Consequently, the wind tunnel data are first corrected to account for variations in the average gap δ_o, so that the prediction of the attitude effect can be isolated. The dependence of both the pitching moment coefficient and the lift coefficient with δ_o, or r_o at constant attitude is shown to be linear and insensitive to $\bar{\alpha}$ in Reference 1; and therefore, the correction to the experimental data is made in the following fashion.

Consider the lift coefficient (the same analysis applies to the pitching moment coefficient) which is a function of three dimensionless parameters

$$C_L = C_L\ (\bar{\alpha},\ r_o,\ r_1)$$

where

$$r_o = \frac{2\delta_o}{W\alpha}$$

$$r_1 = \frac{2\delta_1}{W\alpha}$$

$$\bar{\alpha} = \frac{Wc\alpha}{A_E}$$

The variation, δr_o, with attitude involves a term due to the change in gap and one due to the change in pitch attitude, and the correction is applied to remove the effect of gap change so that

$$\delta r_o = \Delta r_o + \frac{\partial r_o}{\partial \theta} \Delta\theta$$

where

$$\Delta r_o = r_o^* - r_o$$

The value of the attitude at a particular test condition is θ_t and r_o^* is defined as

$$r_o^* \equiv r_o \ (\theta = 0)\frac{\alpha \ (\theta = 0)}{\alpha \ (\theta = \theta_t)}$$

that is, r_o^* is the value of r_o which would be present if the winglet gap at the reference point, at the attitude θ_t, were identical to the gap at $\theta = 0$.

Thus the lift coefficient variation is expressed as

$$C_L = C_{L_{\theta=0}} + \frac{\partial C_L}{\partial \theta} (\theta_t - \theta) + \frac{\partial C_L}{\partial r_o} (r_o^* - r_o) .$$

The last term in this expression represents the term which was calculated in order to determine the correction to be applied to the data to remove the effect of average gap variation. A similar formulation applies to the pitching moment coefficient.

4.1 WIND TUNNEL DATA

As described above, the wind tunnel data are first corrected for gap variation. The experimental values of the variation of pitching moment coefficient and lift coefficient with gap, r_o from Reference 1 are

TABLE 3. CORRECTION OF WIND TUNNEL DATA TO REMOVE AVERAGE GAP (δ_0) EFFECT

	$\bar{\alpha}$	r_1	r_0	r_0^*	Δr_0	ΔC_L	ΔC_M	
1-LEVEL	1.29	0	0.49	-	-	-	-	
1-NOSE UP	1.49	-0.74	0.57	0.45	-0.12	0.033	0.0048	$\Delta C_L = \frac{\partial C_L}{\partial r_0} \Delta r_0$
1-NOSE DOWN	1.11	0.88	0.73	0.54	-0.19	0.051	0.0078	$\Delta C_m = \frac{\partial C_m}{\partial r_0} \Delta r_0$
2-LEVEL	1.36	0	0.54	-	-	-	-	
2-NOSE UP	1.58	-0.80	0.50	0.50	0	0	0	
2-NOSE DOWN	1.12	0.96	0.84	0.60	-0.24	0.065	0.0096	

$\frac{\partial C_L}{\partial r_0} = -0.27$

$\frac{\delta C_M}{\delta r_0} = -0.04$

r_0^* = VALUE OF r_0 WITH ATTITUDE CHANGE ONLY (δ_0 = CONST)

$\Delta r_0 = r_0^* - r_0$

(REFERENCE 1)

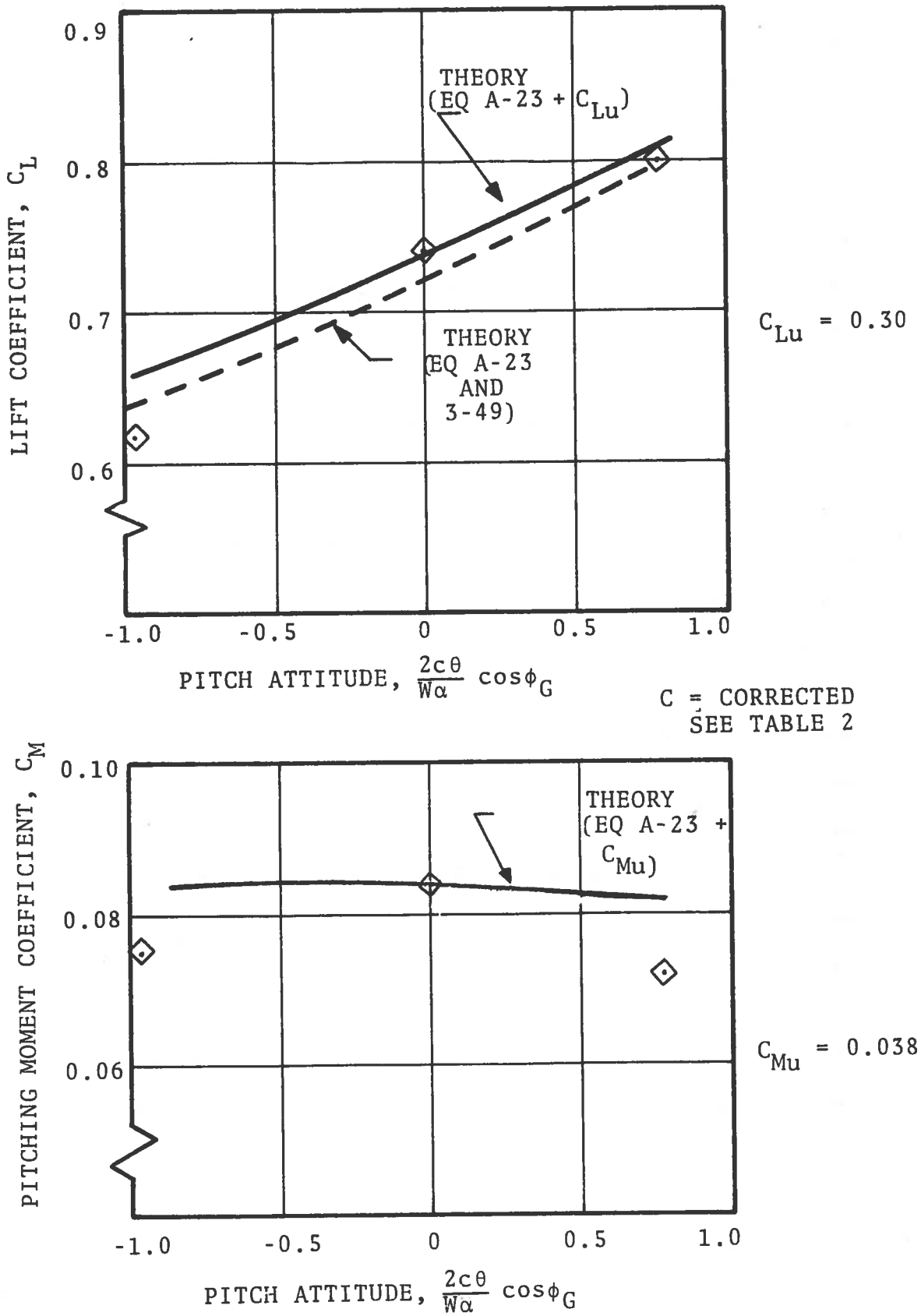

FIGURE 25. COMPARISON OF THEORY AND EXPERIMENT, WIND TUNNEL TEST ($\bar{\alpha}$ = 1.36, r_o = 0.54 at θ = 0) (CONTINUED)

The theory is shown with a constant increment added to match at zero attitude and essentially indicates near zero slope and does not account for the small nonlinearity shown by the experimental data. It would be expected that this non-linear behavior would not be particularly important in a dynamics analysis unless the center of gravity were located at the 50 percent chord point. Appendix D discusses the equations of motion and the influence of center of gravity position on stability. Recall that the pitch/heave dynamics are coupled and the static stability cannot be judged from the pitching moment variation with attitude alone as shown in Appendix D. Note that location of the center of gravity at 50 percent chord may not result in a trimmed vehicle since center of pressure is located near the 40 percent chord point as shown in Section 2. The contribution of the lift variation with attitude would thus tend to linearize the pitching moment variation with attitude if the center of gravity is located at the 40 percent chord point and consequently the agreement between theory and experiment for the pitching moment coefficient is considered quite satisfactory. The theory indicates, as in the case of the lift coefficient, that the effect of $\bar{\alpha}$ is significant; and, in fact, each term in the pitching moment expression (equation (A-23)) contributes to the variation, so that it is difficult to say how well each of the individual effects is predicted.

A further comparison of theory and experiment is shown in Figure 26 where the lower surface contribution to lift and pitching moment coefficient, as predicted by the theory of Appendix A, is compared with the integration of the pressure coefficient measurement along the guideway. The discrepancy in magnitude in each case is similar to that found in Reference 1. The slope

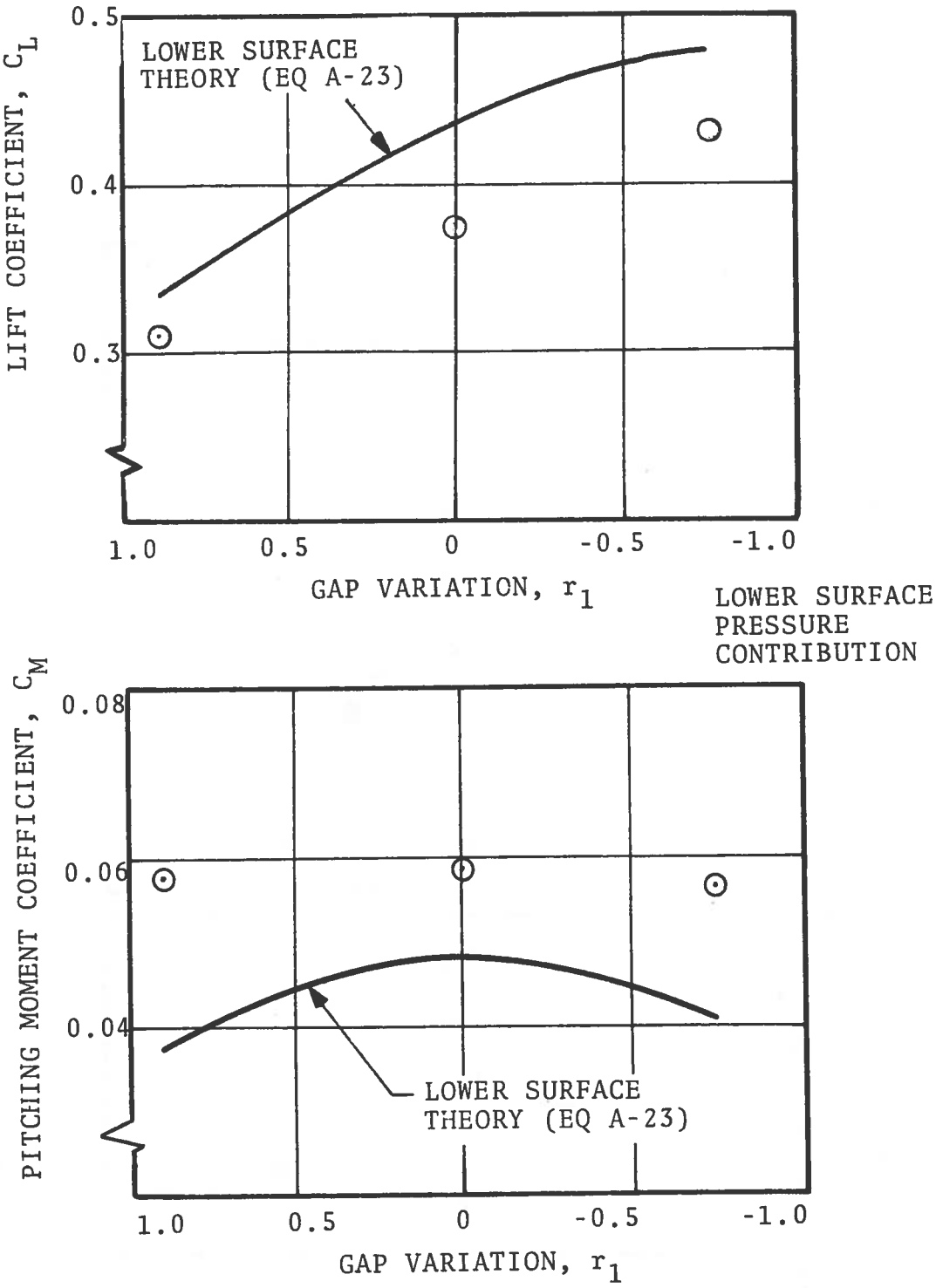

FIGURE 26. COMPARISON OF THEORY AND EXPERIMENT, LOWER SURFACE ONLY, WIND TUNNEL TEST (α = 1.29, r_o = 0.49 at θ = 0)

the nonlinearity present. The wind tunnel experiments appear to indicate somewhat lower slopes than the towed-model data. This difference is no doubt in part due to the fact that the towed-model data are effectively linearized by the method used to analyze the data, which also would account for some of the apparent scatter in the towed-model test results. In particular, the nonlinearities in the pitching moment coefficient data shown in the wind tunnel may add to the difficulty of determining effective linear derivatives. Also, the process of determining the towed model attitude derivatives depends upon evaluation of the height derivatives, i.e., the method of calculating the attitude derivatives is somewhat indirect.

4.3 MOVING MODEL DATA

Comparison of the moving-model data with theory is shown in Figure 28. As in the case of the wind tunnel experiments it was not possible to maintain the average gap constant due to the difficulty in making the small adjustments in model attitude with respect to the guideway. Consequently, in order to compare the effects of pitch attitude obtained from the experiments with theory the effect of average gap changes was corrected for using the same parameter variations with average gap as in the wind tunnel tests. The corrections applied to the data are noted in Table 4 and each point which has been corrected is denoted by a "c" on Figure 28.

The lower surface theory of Appendix A gives reasonable agreement for the variation of lift coefficient with pitch attitude. There does appear to be a non-linearity in lift indicated at the larger nose down attitudes not predicted by the theory. A similar trend can be noted in the wind tunnel results.

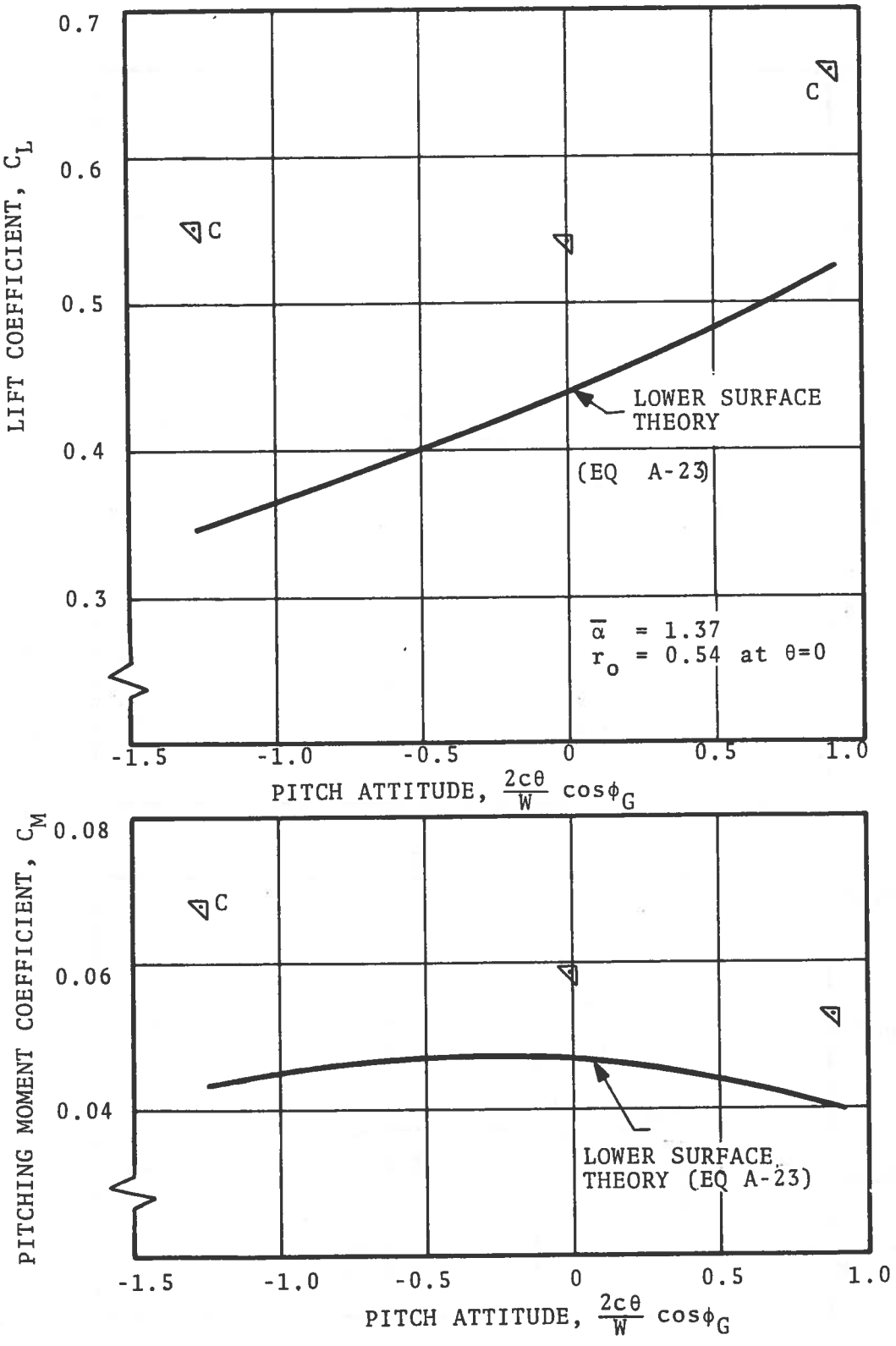

FIGURE 28. COMPARISON OF THEORY AND EXPERIMENT, MOVING MODEL TEST

The theory for the pitching moment variation agrees especially in the nose up case. Similar to the lift coefficient there is a discrepancy in the large nose down condition.

The fact that the slopes are reasonably well predicted tends to indicate that the differences between the wind tunnel data and the moving model data are a result of the loss in lift due to thickness as a result of upper surface separation. The theory indicates that upper surface lift due to thickness does not contribute to force and moment variations with attitude.

Comparison of the total lift coefficient to the prediction based on the lower surface theory of Appendix A indicates that the upper surface is producing a lift coefficient of about 0.1. This contribution agrees with the leading edge effect predicted in Section 3 supporting the notion that separation has occurred and no lift due to thickness is developed.

Further investigation of the aerodynamic effects of the idler carriage and support on the upper surface lift appears highly desirable. It is difficult to design an idler carriage providing the necessary rigidity for the moving model tests without some structure close to the model.

Indications from the comparison of theory and experiment discussed above are that the lower surface pressure distribution is unaffected by the idler carriage.

The overall results of this study and those of Reference 1 indicate that the theory presented in Appendix A is quite satisfactory for predicting the static stability derivatives of a tracked ram air cushion vehicle.

the data are presented referenced to the 50 percent chord of the vehicle where the linear slope is near zero. For a reasonable center-of-gravity location on the vehicle, the lift variation with attitude would tend to linearize this variation.

The steady-state theory indicates that for the center-of-gravity locations in the vicinity of the center of pressure (40 percent chord), the configuration studied will be statically stable in attitude.

Comparison of the upper and lower surface theories indicate that the primary contributions to the vehicle stability derivatives arise from the lower surface contributions. Comparisons of lower surface theory with pressure distributions indicate similar results to those of Reference 1. The lower surface theory indicates a somewhat larger lift contribution than is indicated by the pressure distribution and a center of pressure that is further aft than the pressure distributions indicate. However, the discrepancy in the location of the center of pressure is less than two percent chord.

A theory is presented for the rate dependent effects which indicates that the vehicle aerodynamics give rise to pitch and heave damping.

7. REFERENCES

1.) Curtiss, H.C., Jr. and Putman, W.F.: "Experimental Investigation of Aerodynamic Characteristics of a Tracked Ram Air Cushion Vehicle," Report No. DOT-TSC-OST-78-1 (PB 277674), January 1978.

2.) Barrows, T.M., Widnall, S.E. and Richardson, H.H.: "The Use of Aerodynamic Lift for Application to High Speed Ground Transportation," Report No. DOT-TSC-FRA-71-7 (PB 210 743), June 1971.

3.) Abbott, I.H. and von Doenhoff, A.E.: THEORY OF WING SECTIONS, Dover Publications, New York, 1959.

4.) Lee, S.E.: "A Theoretical Investigation of the Aerodynamic Characteristics of a Tracked Ram Air Cushion Vehicle," Princeton University, Department of Aerospace and Mechanical Sciences Report No. 1255-T, December 1975.

5.) Barrows, T.M.: "Analytical Studies of the Lift and Roll Stability of a Ram Air Cushion Vehicle," DOT-TSC-FRA-72-1 (FRA-RT-73-21), (PB 219 820), December 1972.

6.) Milne-Thompson, L.M.: THEORETICAL HYDRODYNAMICS, MacMillan Co., New York, 1960.

7.) Ashley, H. and Landahl, M.: AERODYNAMICS OF WINGS AND BODIES, Addison-Wesley, Reading, MA, 1965.

8.) Van Dyke, M.: PERTURBATION METHODS IN FLUID MECHANICS, Academic Press, New York, 1964.

9.) Van Dyke, M.: "Second-Order Slender Body Theory - Axisymmetric Flow," NASA Technical Report No. R-47, 1959.

10.) Boccadoro, T.A.: "Towing Tank Tests on a Ram Wing in a Rectangular Guideway," Report No. DOT-TSC-FRA-73-81 (FRA-RT-73-34), (PB 222 476/4), July 1972.

11.) Luhrs, R.A., Sweet, L.M. and Curtiss, H.C., Jr.: "A Comparative Study of the Ride Quality of TRACV Suspension Alternatives," Report No. DOT-TSC-RSPA-78-23, (PB 297840), June 1979

APPENDIX A

THEORY FOR PITCH ATTITUDE AERODYNAMICS

In Reference 1 a theory is presented for the prediction of the lift, drag and pitching moment of a tracked ram air cushion vehicle. The theory is a simplified version of a theory developed by Boccadoro[10] which involves a one-dimensional approximation of the flow field under the vehicle. This theory was developed for the case in which the side gap is constant along the length of the vehicle and thus considers only the effect of the height of the vehicle above the guideway. Reference 1 shows that this theory agrees well with experimental data, especially with respect to predicting the stability derivatives of the vehicle.

In order to develop a complete description of the aerodynamics of the tracked ram air cushion vehicle the theory must be extended to include the influence of pitch attitude, which will result in a side gap that varies linearly along the length of the vehicle.

Figure A-1 shows the nomenclature for the theory. The continuity equation written for the control volume shown in the figure can be expressed as follows,

$$\rho A_L U = \rho A_E U_E + 2 \rho \int_x^c \delta w \, d\xi \qquad \text{(A-1)}$$

It has been assumed that the velocities U and U_E are uniform across their respective areas. The velocity at the gap, w, is assumed to be only a function of distance along the body, x, and uniform across the width of the gap. Assuming that the flow is incompressible, the density cancels out of equation (A-1).

The area variation along the body is still taken to have a linear variation with distance along the body as is characteristic of the model used in the experiments. The side gap is also considered to have a linear variation along the length of the body. The area and the gap are given as functions of x as

$$A_L = A_E + Wc\alpha\left(1 - \frac{x}{c}\right) \tag{A-6}$$

$$\delta = \delta_o + \delta_1\left(\frac{x}{c} - \frac{x_o}{c}\right) \tag{A-7}$$

as shown in Figure A-2. In terms of the gap at the leading and trailing edge of the vehicle

$$\begin{aligned} \delta_o &= \delta_{TE}\,\bar{x}_o + \delta_{LE}\,(1 - \bar{x}_o) \\ \delta_1 &= \delta_{TE} - \delta_{LE}\ . \end{aligned} \tag{A-8}$$

The pitch attitude of the vehicle is defined with respect to the vehicle trim condition in which the winglets are parallel to the guideway. In this condition, the slope of the lower surface of the vehicle is α_o, so that the dependence of the flow under the vehicle on pitch attitude is found from the relationships

$$\begin{aligned} \alpha &= \alpha_o + \theta \\ \theta &= \frac{\delta_{LE} - \delta_{TE}}{c\cos\phi_G} = -\frac{\delta_1}{c\cos\phi_G}\ . \end{aligned} \tag{A-9}$$

Relationship (A-7) is substituted into the differential equation and the various equations are nondimensionalized using the exit area, A_E, free stream velocity, U, and vehicle length, c:

$$\frac{d(\bar{A}\bar{U})}{d\bar{x}} = -\,\bar{\alpha}\,\{r_o + r_1\,(\bar{x} - \bar{x}_o)\}\sqrt{1 - \bar{U}^2}\ . \tag{A-10}$$

The solution for small r is obtained therefore, by neglecting f on the right hand side of equation (A-12). The equation can be readily integrated to give

$$f = \{r_o + \frac{r_1}{\bar{\alpha}} (1 + \bar{\alpha} (1 - \bar{x}_o)) (\lambda - \tan^{-1}\lambda) - \frac{r_1}{\bar{\alpha}} \{ \frac{\lambda\sqrt{\lambda^2 + 1}}{2} - \frac{1}{2} \ln (\lambda + \sqrt{\lambda^2 + 1}) . \tag{A-13}$$

With this solution, the pressure coefficient on the lower surface and consequently the lift and pitching moment coefficients can be calculated. The pressure coefficient is given by

$$C_p \cong \frac{\lambda^2 - 2f}{\lambda^2 + 1} . \tag{A-14}$$

Consistant with the approximate solution to the differential equations, f^2 has been neglected. The lift and pitching moment coefficients are given by,

$$C_L = \int_o^1 C_p \, d\bar{x} \tag{A-15}$$

$$C_M = - \int_o^1 C_p (\bar{x} - \bar{x}_o) \, d\bar{x}$$

The pitching moment coefficient may also be written as

$$C_M = - \int_o^1 C_p \, \bar{x} \, d\bar{x} + C_L \, \bar{x}_o . \tag{A-16}$$

In terms of the variable λ,

$$C_L = - \frac{1}{\bar{\alpha}} \int_{\lambda_o}^{o} C_p \left(\frac{\lambda d\lambda}{\sqrt{\lambda^2 + 1}}\right) \tag{A-17}$$

$$C_M = \frac{1}{\bar{\alpha}} \int_{\lambda_o}^{o} C_p \left(\frac{\bar{\alpha} + 1}{\bar{\alpha}} - \frac{\sqrt{\lambda^2 + 1}}{\bar{\alpha}}\right) \frac{\lambda d\lambda}{\sqrt{\lambda^2 + 1}} + C_L \, \bar{x}_o . \tag{A-18}$$

$$F_{3L} = \lambda_o - 2 \tan^{-1}\lambda_o + \frac{\ln\left(\lambda_o + \sqrt{\lambda_o^2 + 1}\right)}{\sqrt{\lambda_o^2 + 1}} \qquad \text{(A-21)}$$

$$F_{1M} = \frac{\bar{\alpha}}{2}(2 + \bar{\alpha}) - \ln(1 + \bar{\alpha})$$

$$F_{2M} = \lambda_o - \tan^{-1}\lambda_o - \int_o^{\lambda_o} \frac{\lambda \tan^{-1}\lambda \, d\lambda}{\lambda^2 + 1}$$

$$F_{3M} = \frac{\lambda_o\sqrt{\lambda_o^2 + 1}}{2} - \frac{1}{2}\ln\left(\lambda_o + \sqrt{\lambda_o^2 + 1}\right) - \int_o^{\lambda_o} \frac{\lambda \ln\left(\lambda + \sqrt{\lambda^2 + 1}\right) d\lambda}{(\lambda^2 + 1)}$$

where $\lambda_o = [(1 + \bar{\alpha})^2 - 1]^{1/2}$

The terms with integral signs cannot be integrated exactly and therefore are calculated on a digital computer. Alternatively, the substitution $y^2 = \lambda^2 + 1$ reduces these two integrals to tabulated forms, both having series solutions.

A second set of functions related to the F's is defined,

$$L_1(\bar{\alpha}) = \frac{F_{1L}}{\bar{\alpha}} \qquad M_1(\bar{\alpha}) = \frac{F_{1M}}{\bar{\alpha}^2}$$

$$L_2(\bar{\alpha}) = \frac{2F_{2L}}{\bar{\alpha}} \qquad M_2(\bar{\alpha}) = \frac{2F_{2M}}{\bar{\alpha}^2} \qquad \text{(A-22)}$$

$$L_3(\bar{\alpha}) = \frac{F_{3L} - 2F_{2L}}{\bar{\alpha}^2} \qquad M_3(\bar{\alpha}) = \frac{F_{3M} - 2F_{2M}}{\bar{\alpha}^3}$$

The resulting equations for the lift coefficient and pitching moment coefficient are

$$C_L = L_1 - r_o L_2 + r_1(\bar{x}_o - 1) L_2 + r_1 L_3 \qquad \text{(A-23)}$$

$$C_M = C_L\left(\bar{x}_o - \frac{\bar{\alpha} + 1}{\bar{\alpha}}\right) + M_1 - r_o M_2 + r_1(\bar{x}_o - 1) M_2 + r_1 M_3$$

and these dimensionless quantities are related to the height and attitude of the vehicle by

$$\begin{aligned} \alpha &= (\alpha_o + \theta) \\ A_E &= A_{SE} + [h - (\theta + \alpha_o)(c - x_o)]\, W \\ \delta_1 &= - c\, \theta \cos \phi_G \quad . \end{aligned} \tag{A-25}$$

A_{SE} is the part of the exit area due to lateral spacing between the body and the trailing edge.

The variation of C_L and C_M with h and θ is to be determined. It is assumed here that the initial attitude of the vehicle, θ, is zero and in addition that the winglets are rigidly attached to the vehicle so that

$$\frac{d\delta_o}{dh} = \cos \varphi_G$$

The height derivatives are,

$$\begin{aligned} \frac{dC_L}{d\bar{h}}\bigg|_\theta &= \frac{\partial C_L}{\partial \bar{\alpha}} \frac{d\bar{\alpha}}{d\bar{h}} + \frac{\partial C_L}{\partial r_o} \frac{dr_o}{d\bar{h}} \\ \frac{dC_M}{d\bar{h}}\bigg|_\theta &= \frac{\partial C_M}{\partial \bar{\alpha}} \frac{d\bar{\alpha}}{d\bar{h}} + \frac{\partial C_M}{\partial r_o} \frac{dr_o}{d\bar{h}} \quad . \end{aligned} \tag{A-26}$$

Note that $\dfrac{dr_1}{d\bar{h}} = 0$

$$\begin{aligned} \frac{dr_o}{d\bar{h}} &= \frac{2c}{W\alpha_o} \cos \phi_G = \frac{2}{AR\alpha_o} \cos \phi_G \\ \frac{d\bar{\alpha}}{d\bar{h}} &= - \frac{\bar{\alpha}^2}{\alpha_o} \quad . \end{aligned} \tag{A-27}$$

The initial value of r_1 is taken to be zero

$$C_M = M_1 - r_o M_2 + r_1 [(\bar{x}_o - 1) M_2 + M_3] + C_L [\bar{x}_o - \frac{\bar{\alpha} + 1}{\bar{\alpha}}] \qquad \text{(A-23)}$$

and therefore

$$\frac{\partial C_M}{\partial \bar{\alpha}} = \frac{\partial M_1}{\partial \bar{\alpha}} - r_o \frac{\partial M_2}{\partial \bar{\alpha}} + \frac{\partial C_L}{\partial \bar{\alpha}} (\bar{x}_o - \frac{\bar{\alpha} + 1}{\bar{\alpha}}) + \frac{1}{\bar{\alpha}^2} C_{L_o}$$

$$\frac{\partial C_M}{\partial r_o} = - M_2 + \frac{\partial C_L}{\partial r_o} (\bar{x}_o - \frac{\bar{\alpha} + 1}{\bar{\alpha}}) \qquad \text{(A-33)}$$

$$\frac{\partial C_M}{\partial r_1} = (\bar{x}_o - 1) M_2 + M_3 + \frac{\partial C_L}{\partial r_1} (\bar{x}_o - \frac{\bar{\alpha} + 1}{\bar{\alpha}}) \quad .$$

Thus, equations (A-28) and (A-31) give the four static stability derivatives. Given a vehicle trim condition, using equations (A-32) and (A-33) these four derivatives can be calculated. These results, taken with those of Appendix B, determine the aerodynamic stability derivatives required to develop the equations of motion of a TRACV.

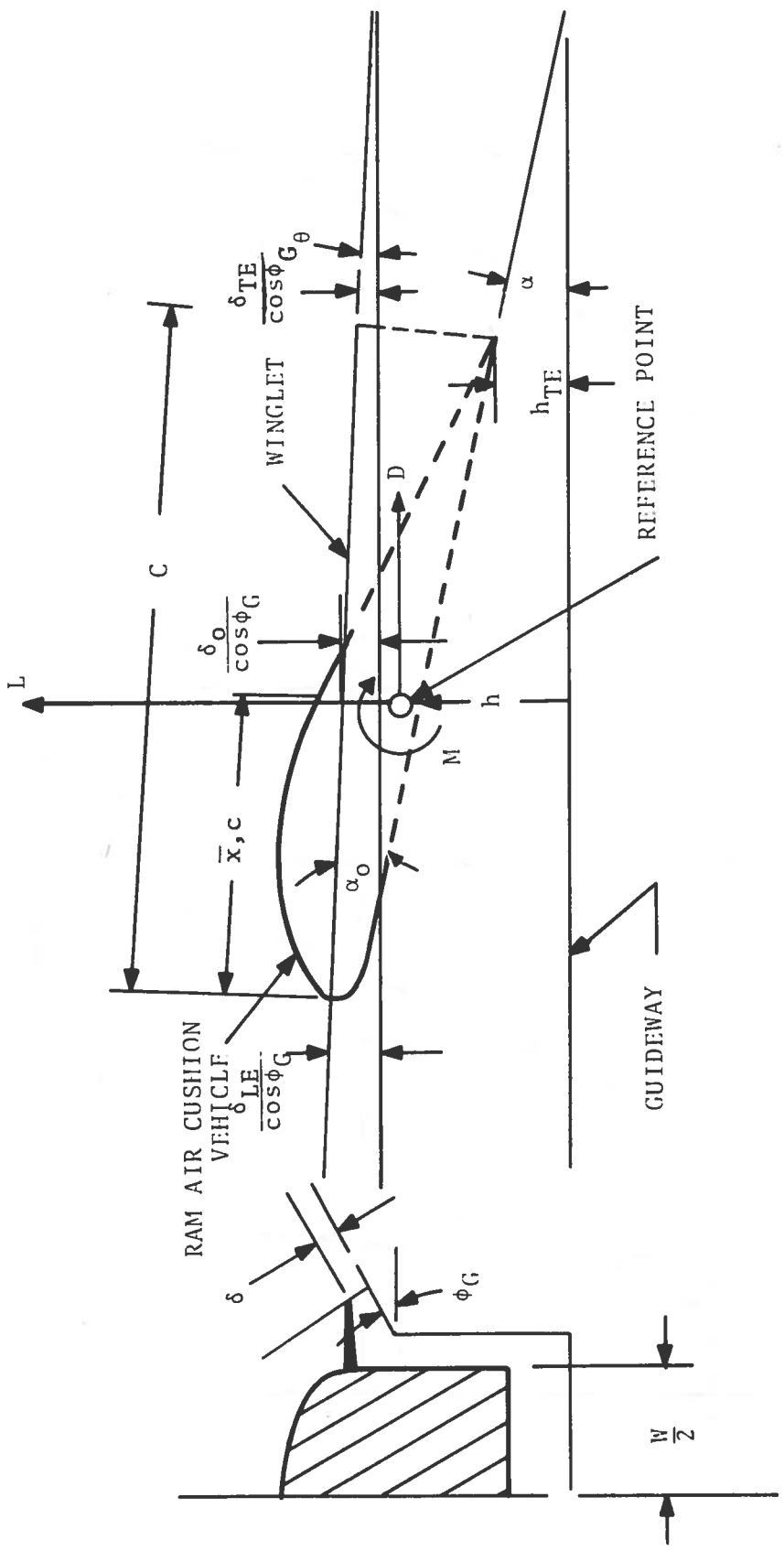

FIGURE A-2. GEOMETRY FOR ATTITUDE THEORY

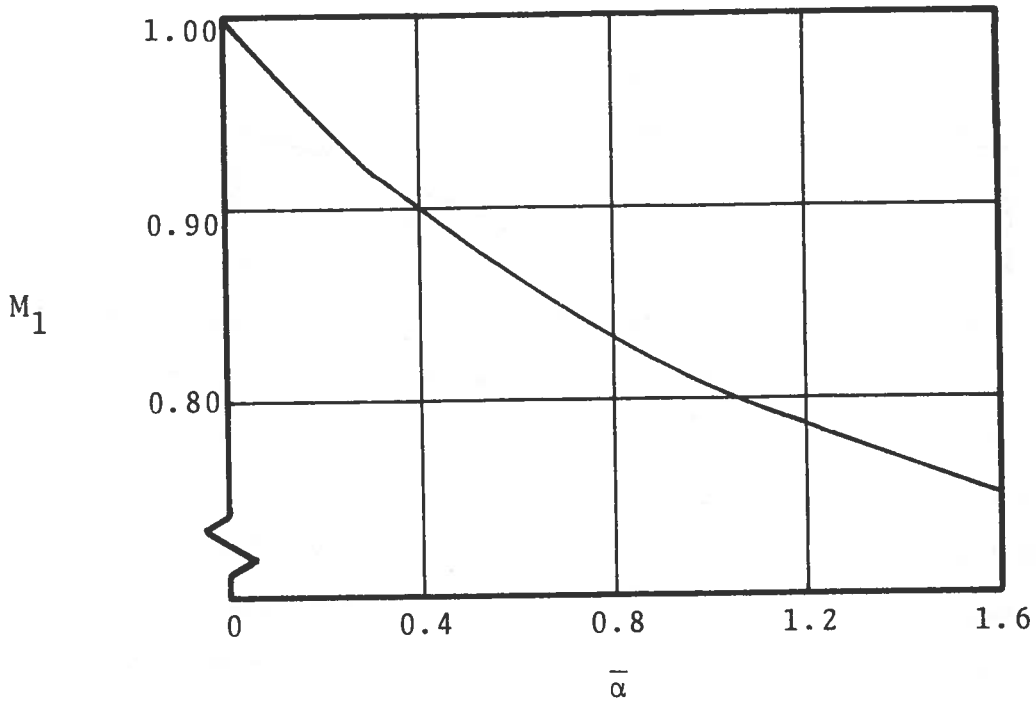

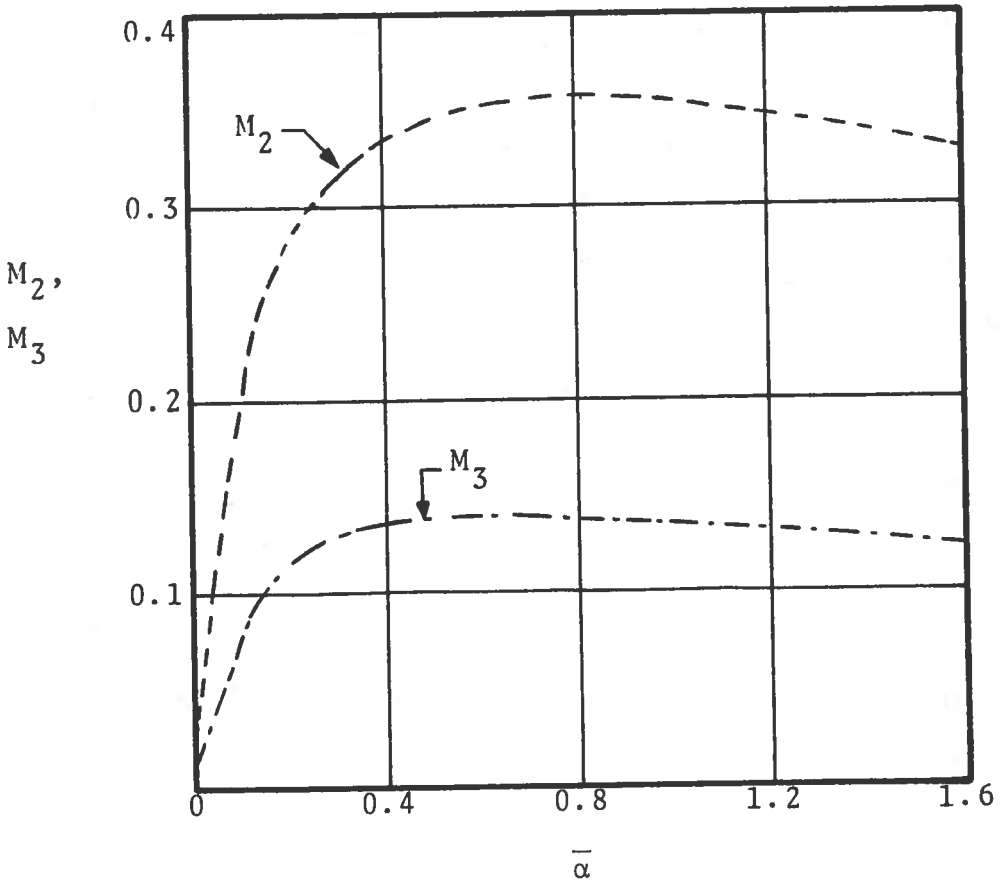

FIGURE A-3. LIFT AND PITCHING MOMENT FUNCTIONS (CONTINUED)

$$\frac{df}{d\lambda} = \frac{\lambda}{\lambda^2 + 1}\{r\,(\lambda^2 - 2f - f^2)^{1/2}\} - \frac{\lambda}{\sqrt{\lambda^2 + 1}}\left[(\bar{x} - \bar{x}_o)\,\frac{D\theta}{\alpha} - \frac{D\bar{h}}{\alpha}\right] \qquad \text{(B-5)}$$

where

$$(\bar{x} - \bar{x}_o) = 1 + \frac{1}{\bar{\alpha}} - \bar{x}_o - \frac{\sqrt{\lambda^2 + 1}}{\bar{\alpha}} \quad .$$

The first group of terms on the right hand side of equation (B-5) represent the steady flight solution and this part of the equation was solved in Appendix A. Since this solution involved solving equation (B-5) by neglecting the terms in f on the right hand side, the influence of the rate terms may be calculated as an increment to the solution of Appendix A.

Thus, the increment in f due to vertical velocity and angular rate, Δf, is given by

$$\frac{d\Delta f}{d\lambda} = -\frac{1}{\alpha}\frac{\lambda}{\sqrt{\lambda^2 + 1}}\{(1 + \frac{1}{\bar{\alpha}} - \bar{x}_o - \frac{\sqrt{\lambda^2 + 1}}{\bar{\alpha}})\,D\theta - D\bar{h}\} \qquad \text{(B-6)}$$

The boundary condition is $f(0) = 0$. This equation can be readily integrated to give,

$$\Delta f = -\frac{1}{\alpha}\left((1 + \frac{1}{\bar{\alpha}} - \bar{x}_o)\,D\theta - D\bar{h}\right)\left(\sqrt{\lambda^2 + 1} - 1\right) + \frac{D\theta}{\alpha\bar{\alpha}}\,\frac{\lambda^2}{2} \quad . \qquad \text{(B-7)}$$

The calculation of the increment in lift and pitching moment coefficient follow from Appendix A and can be expressed as

$$\Delta C_L = \frac{2Wc}{A_E\,\bar{\alpha}^2}\left[\ln\,\frac{1}{1 + \bar{\alpha}} + \frac{\bar{\alpha}}{1 + \bar{\alpha}}\right] D\bar{h}$$

$$- \frac{Wc}{A_E\,\bar{\alpha}^2}\left[2(1 + \frac{1}{\bar{\alpha}} - \bar{x}_o)\,(\ln\,\frac{1}{1 + \bar{\alpha}} + \frac{1}{1 + \bar{\alpha}}) + \frac{\bar{\alpha}}{1 + \bar{\alpha}}\right] D\theta \qquad \text{(B-8)}$$

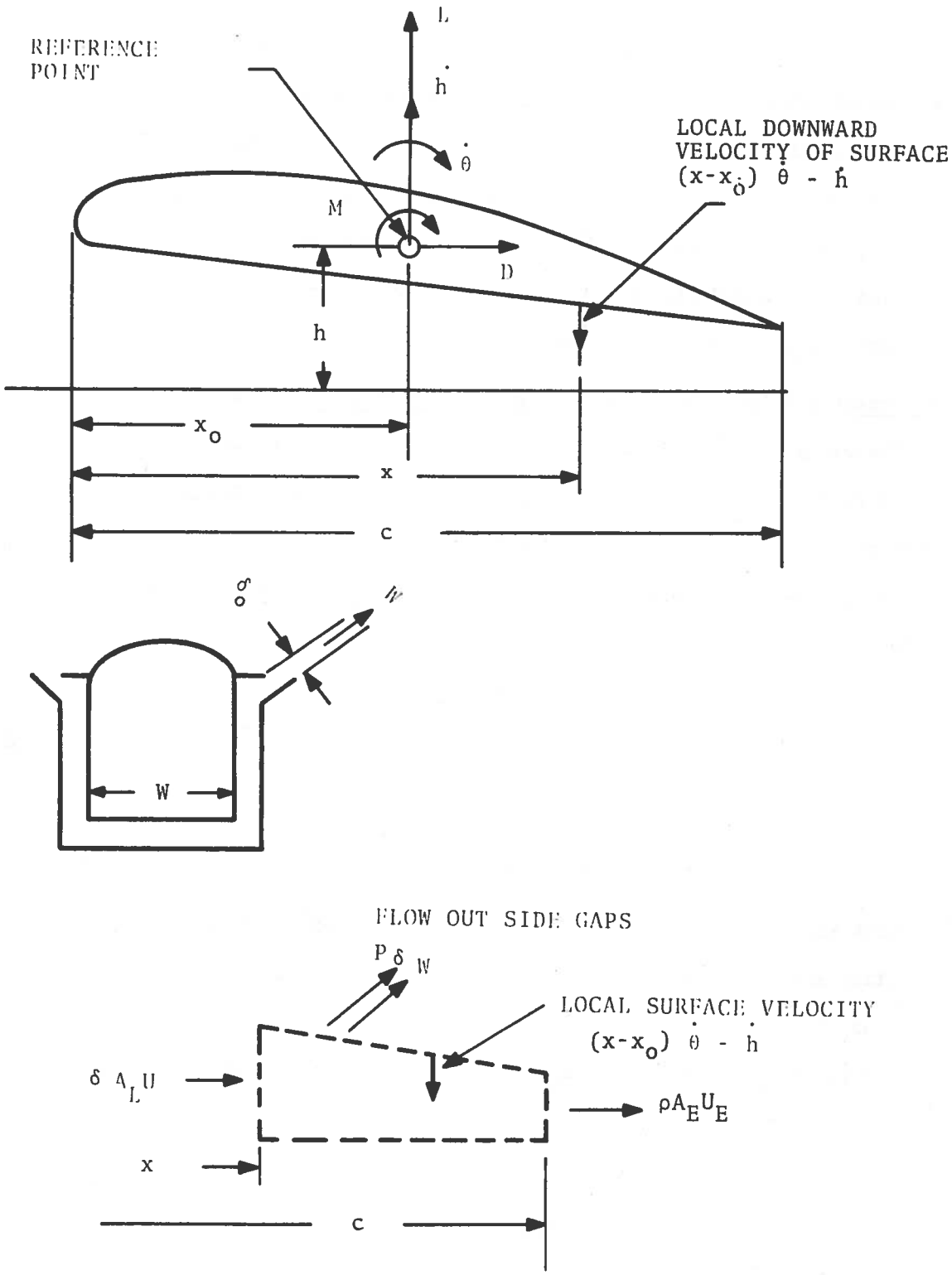

FIGURE B-1. NOMENCLATURE AND GEOMETRY FOR RATE DERIVATIVE THEORY

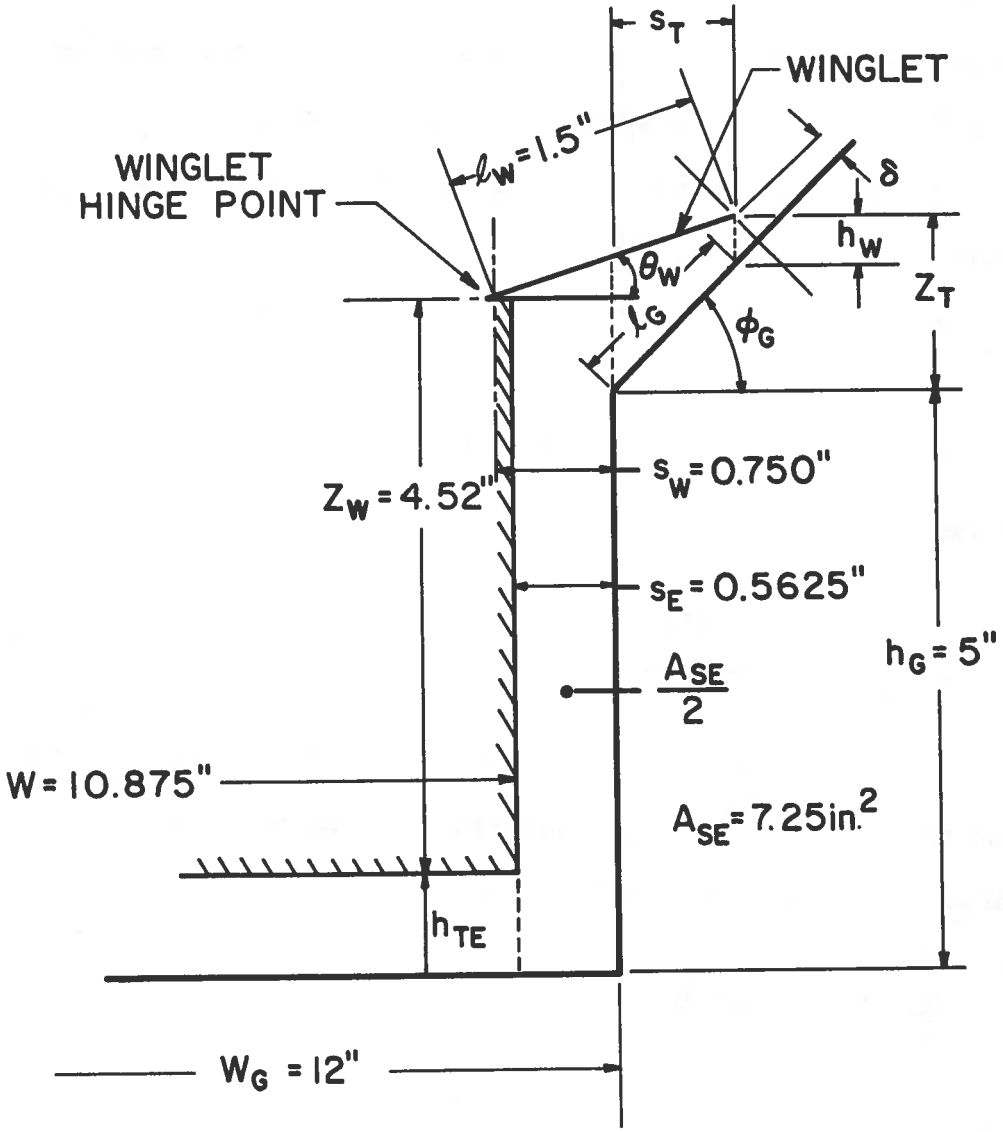

FIGURE C-1. DETAILED GEOMETRY OF WINGLET AND GUIDEWAY

The latter derivative may also be expressed in terms of winglet rotation as

$$\left.\frac{dL}{d\theta_w}\right|_h = e' \cos \phi_G \left.\frac{dL}{d\delta}\right|_h \quad .$$

Similar relationships hold for the pitching moment derivatives.

If the winglet is held fixed with respect to the body, i.e., a rigid vehicle is considered, then

$$\Delta\theta_w = 0$$

and the winglet gap perturbation is related to a vehicle height perturbation by the relationship

$$\Delta\delta = \Delta h_{TE} \cos \phi_G \quad ,$$

and therefore, the heave derivative for a rigid vehicle is

$$\left.\frac{dL}{dh}\right|_{\theta_w} = \left.\frac{dL}{dh}\right|_{\delta} + \left.\frac{dL}{d\delta}\right|_h \left.\frac{d\delta}{dh}\right|_{\theta_w}$$

$$= \left.\frac{dL}{dh}\right|_{\delta} + \cos \phi_G \left.\frac{dL}{d\delta}\right|_h \quad .$$

In dimensionless form,

$$\left.\frac{dL}{dh}\right|_{\theta_w} = q\,S \left\{\frac{2}{W\alpha} \frac{dC_L}{dr} \cos \phi_G - \frac{\bar{\alpha}^2}{c\alpha} \frac{dC_L}{d\bar{\alpha}}\right\}$$

or as

$$\left.\frac{dL}{dh}\right|_{\theta_w} = \frac{qS}{W\alpha} \left\{2 \frac{dC_L}{dr} \cos \phi_G - \bar{\alpha}^2 \frac{W}{c} \frac{dC_L}{d\bar{\alpha}}\right\} \quad .$$

This is the combination of dimensionless derivatives determined from the towed model tests since the winglet was fixed with respect to the body in these experiments.

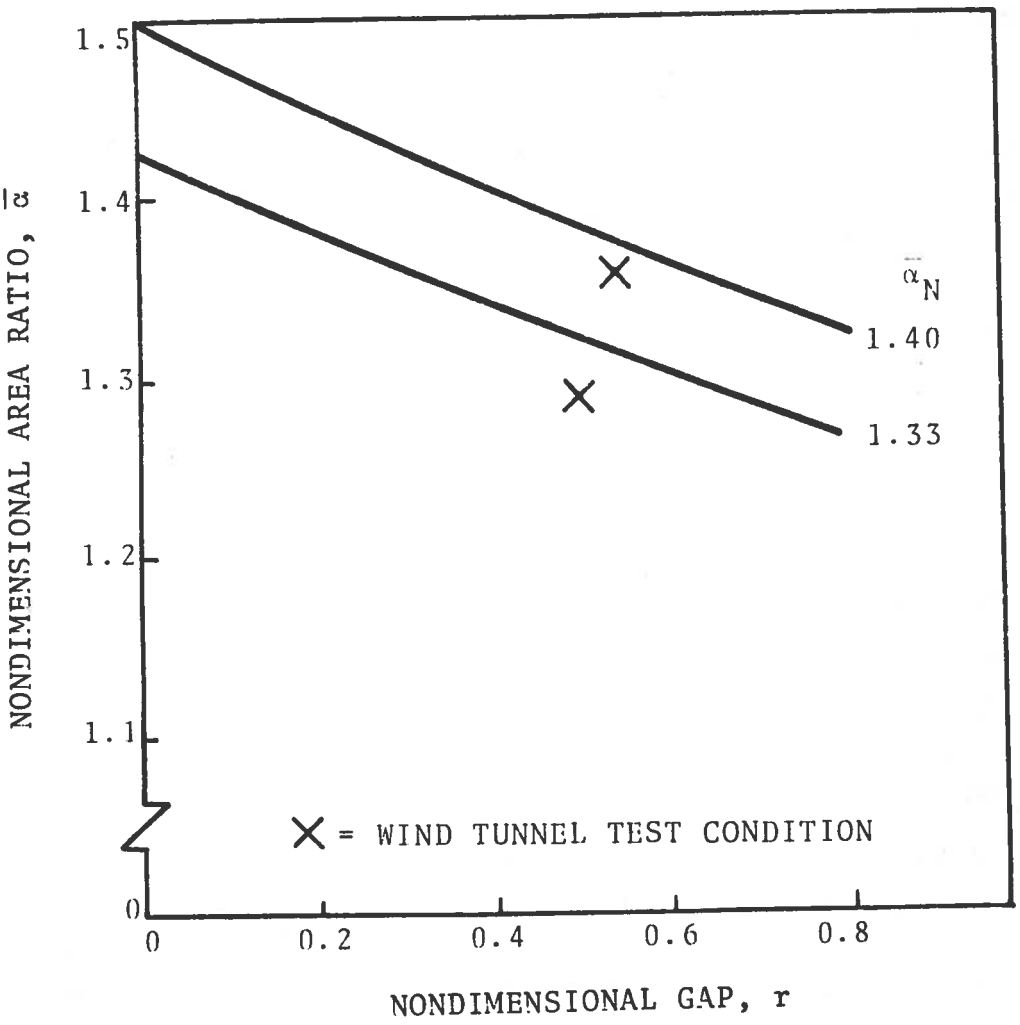

FIGURE C-2. PARAMETER RELATIONSHIPS, TOWED MODEL TESTS

Therefore, along lines of constant center-of-gravity position

$$\frac{\partial C_{\bar{M}}}{\partial r} \Delta r + \frac{\partial C_{\bar{M}}}{\partial \theta} \Delta\theta = 0 \ ,$$

and therefore,

$$\left.\frac{\Delta\theta}{\Delta r}\right|_{CG} = - \frac{\frac{\partial C_{\bar{M}}}{\partial r}}{\frac{\partial C_{\bar{M}}}{\partial \theta}} \ .$$

That is, the variation of attitude with gap is a direct measure of the ratio of the pitching moment derivatives in equilibrium flight at different lift coefficients. Thus, the location of the center of grav essentially determines the attitude and gap variation which will occu as speed is changed.

At a different center-of-gravity position

$$C_{M_{CG2}} = C_{M_{CG1}} + \Delta\bar{x}\, C_L \ .$$

In equilibrium flight, $C_{M_{CG2}} = 0$, and therefore, at constant lift coefficient the change in the pitching moment coefficient about posit 1 is

$$\frac{\partial C_{M_{CG1}}}{\partial r} \Delta r + \frac{\partial C_{M_{CG1}}}{\partial \theta} \Delta\theta = - \Delta\bar{x}\, C_L \ .$$

Thus, from the graph of lift coefficient vs. pitching moment coeffici the total quantity on the left hand side can be determined. Finding corresponding points on the equilibrium curve of θ vs. r at the proper lift coefficient determines the change in θ and r to be inserted in above relationship. This result is then employed, along with the rati the derivatives determined from the slope of the equilibrium curve, t

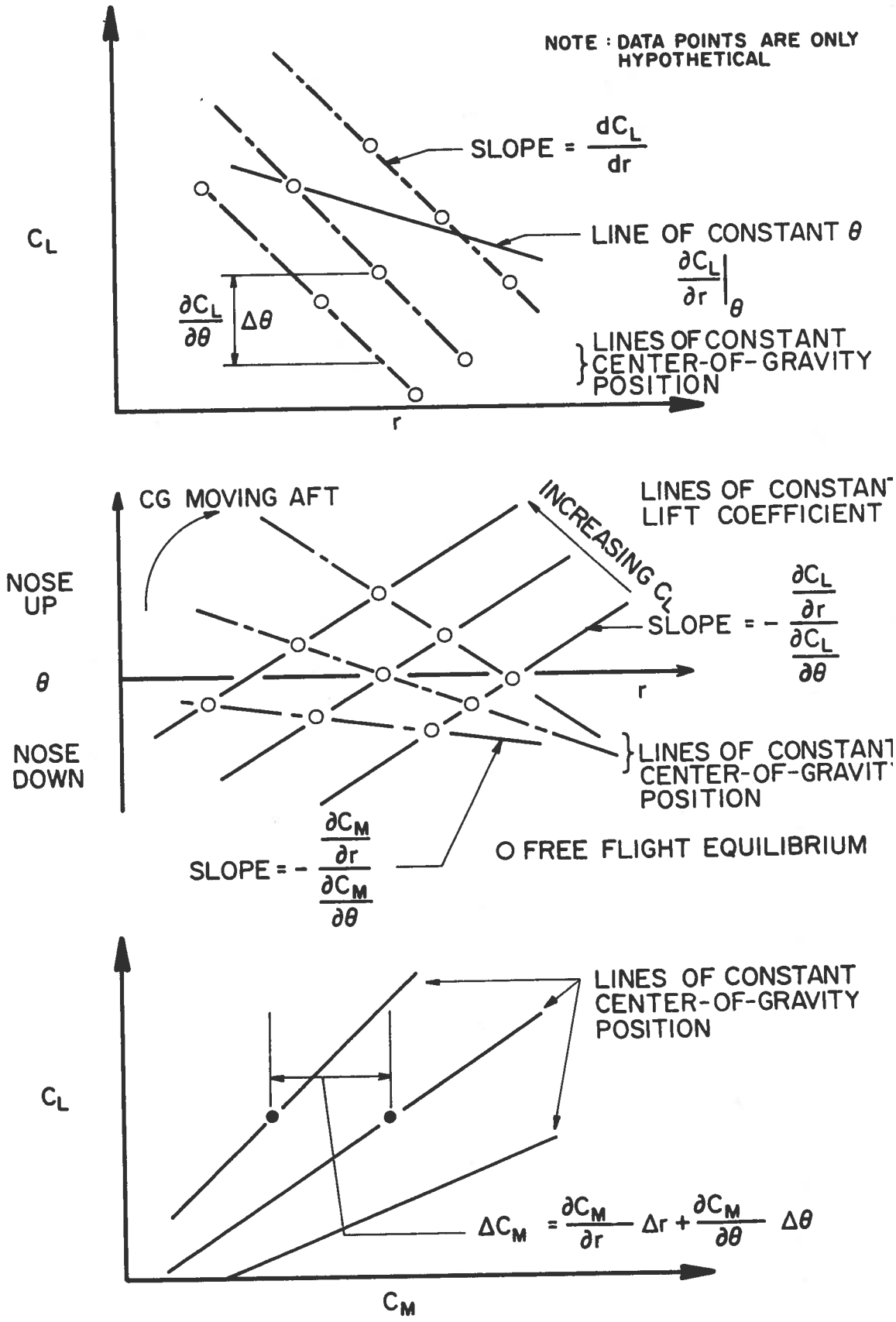

FIGURE C-3. STABILITY DERIVATIVE DETERMINATION, TOWED MODEL TEST

APPENDIX D

EQUATIONS OF MOTION AND STATIC STABILITY

The condition for static stability, i.e., the absence of a real positive root in the characteristic equation describing pitch/heave motion and its dependence upon vehicle center-of-gravity location is examined in this Appendix. The pitch/heave motion is coupled since, in general, both the lift and pitching moment depend upon height and attitude. The speed of the vehicle is assumed to be constant. The equations of motion in a space fixed axis system are

$$\begin{aligned} m\ddot{h} &= L - W', \\ I\ddot{\theta} &= \bar{M}, \end{aligned} \tag{D-1}$$

where h is the vertical displacement of the center of gravity and $\bar{M}$ is the pitching moment about the center of gravity. The aerodynamic lift and pitching moment are expanded in a Taylor series about a trim condition

$$\begin{aligned} L &= L_o + \frac{\partial L}{\partial h} h + \frac{\partial L}{\partial \theta} \theta + \frac{\partial L}{\partial \dot{h}} \dot{h} + \frac{\partial L}{\partial \dot{\theta}} \dot{\theta} , \\ \bar{M} &= \bar{M}_o + \frac{\partial \bar{M}}{\partial h} h + \frac{\partial \bar{M}}{\partial \theta} \theta + \frac{\partial \bar{M}}{\partial \dot{h}} \dot{h} + \frac{\partial \bar{M}}{\partial \dot{\theta}} \dot{\theta} \end{aligned} \tag{D-2}$$

Substituting equations (D-2) into (D-1), the trim or equilibrium condition is given by

$$\begin{aligned} L_o &= W', \\ \bar{M}_o &= 0 . \end{aligned} \tag{D-3}$$

The perturbation equations describing the linearized dynamic motions are

Equation (D-7) is the static stability criterion expressed in terms of stability derivatives referenced to the center of gravity of the vehicle. In the experimental and theoretical studies of this report and Reference 1 the reference location for the pitching moment and vertical displacement is taken to be 50 percent chord. To express the static stability in terms of quantities referenced to this location the following transfer relationships (Figure D-1) are required:

$$\overline{M} = M - L\left(\frac{c}{2} - x_{CG}\right) \tag{D-8}$$

and

$$h = h_{0.5c} + \theta\left(\frac{c}{2} - x_{CG}\right) . \tag{D-9}$$

Thus, the following relationships exist between the derivatives at the 50 percent chord location and an arbitrary center of gravity location x_{CG},

$$L_h = L_{h_{0.5c}}$$

$$L_\theta\Big|_h = L_\theta\Big|_{h_{0.5c}} - L_{h_{0.5c}}\left(\frac{c}{2} - x_{CG}\right)$$

$$\overline{M}_h = M_{h_{0.5c}} - \frac{m}{I}\left(\frac{c}{2} - x_{cg}\right) L_{h_{0.5c}} \tag{D-10}$$

$$\overline{M}_\theta\Big|_h = M_\theta\Big|_{h_{0.5c}} - \frac{m}{I}\left(\frac{c}{2} - x_{CG}\right) L_\theta\Big|_{h_{0.5c}}$$

$$- \left(\frac{c}{2} - x_{CG}\right)\left[M_{h_{0.5c}} - \frac{m}{I} L_{h_{0.5c}}\left(\frac{c}{2} - x_{CG}\right)\right] .$$

the relationships developed above to express

$$-(\bar{M}_\theta + L_h) = -M_{\theta_{0.5c}} + \left(\frac{c}{2} - x_{CG}\right)\left[M_{h_{0.5c}} + \frac{m}{I} L_\theta\Big|_{h_{0.5c}}\right] \qquad \text{(D-13)}$$

$$-\left(1 + \frac{m}{I}\left(\frac{c}{2} - x_{CG}\right)^2\right) L_{h_{0.5c}} > 0 \ .$$

Thus, it can be seen that the center-of-gravity location does influence the dynamic stability through the s^2 term. The influence of moving the center of gravity appears to depend primarily on the sign of the quantity ($M_{h_{0.5c}} + \frac{m}{I} L_\theta\Big|_{h_{0.5c}}$) since the radius of gyration in pitch would be large compared to the distance between the 50 percent chord point and the center-of-gravity location for reasonable trim attitudes. The experimental data indicate that these terms are of opposite sign, i.e., $M_{h_{0.5c}}$ is negative and $L_\theta\Big|_{h=0.5c}$ is positive, so specific vehicle configurations must be studied to evaluate the influence of center-of-gravity position on stability.

It is also interesting to note that the results obtained for the static stability derivatives imply that it is not possible to model the longitudinal dynamics of the TRACV by a simple spring or equivalent two-point suspension model. In general, the coupling terms L_θ and $\bar{M}_h$ are of opposite sign, indicating that there is not a simple equivalent conservative system or spring model that can be used to represent the longitudinal dynamics.

APPENDIX E

REPORT OF NEW TECHNOLOGY

After diligent review of the work performed under this contract, no innovation, discovery, improvement, or invention of a patenable nature was made. The unconventional vehicle configuration which is described herein originated from previous efforts. The main contribution of the present effort was to supply quantitative test data on the dynamics of the concept.

110 copies